Biosensors and Bioelectronics 222 (2023) 114944

Contents lists available at ScienceDirect

Biosensors and Bioelectronics

journal homepage: www.elsevier.com/locate/bios

Recent advances in non-optical microfluidic platforms for bioparticle detection

Bayinqiaoge [a], Yuxin Zhang [a], Tim Cole [a], Jiahao Zheng [a], Jinhong Guo [b,**], Shi-Yang Tang [a,*]

[a] Department of Electronic, Electrical and Systems Engineering, University of Birmingham, Edgbaston, Birmingham, B15 2TT, UK
[b] The M.O.E. Key Laboratory of Laboratory Medical Diagnostics, The College of Laboratory Medicine, Chongqing Medical University, #1 Yixueyuan Road, Yuzhong District, Chongqing, 400016, China

ARTICLE INFO

Keywords:
Microfluidics
Bioparticle detection
Non-optical methods
Point-of-care testing

ABSTRACT

The effective analysis of the basic structure and functional information of bioparticles are of great significance for the early diagnosis of diseases. The synergism between microfluidics and particle manipulation/detection technologies offers enhanced system integration capability and test accuracy for the detection of various bioparticles. Most microfluidic detection platforms are based on optical strategies such as fluorescence, absorbance, and image recognition. Although optical microfluidic platforms have proven their capabilities in the practical clinical detection of bioparticles, shortcomings such as expensive components and whole bulky devices have limited their practicality in the development of point-of-care testing (POCT) systems to be used in remote and underdeveloped areas. Therefore, there is an urgent need to develop cost-effective non-optical microfluidic platforms for bioparticle detection that can act as alternatives to optical counterparts. In this review, we first briefly summarise passive and active methods for bioparticle manipulation in microfluidics. Then, we survey the latest progress in non-optical microfluidic strategies based on electrical, magnetic, and acoustic techniques for bioparticle detection. Finally, a perspective is offered, clarifying challenges faced by current non-optical platforms in developing practical POCT devices and clinical applications.

1. Introduction

Infectious diseases can have a significant impact on the human body, and may also cause a long-lasting impact on the entirety of human society (Bansal, 2020; Pallazola et al., 2019). Recently, the outbreak of the Corona Virus Disease 2019 (COVID-19) global pandemic caused an incredibly large number of lives to be lost worldwide, and presented an unprecedented challenge to global public health (Gautam and Hens, 2020; Harper et al., 2020; Pokhrel and Chhetri, 2021). To alleviate the spread of infectious diseases, it is crucial to make an effective diagnosis, which mainly relies on collecting samples from body fluids such as blood (Lee et al., 2021b), urine (Tai et al., 2021), or saliva (Bellagambi et al., 2020) to test the bioparticles. Bioparticles in these body fluids constantly record the physiological and pathological changes of the human body, and in this sense, the detection of bioparticles is clinically significant for improving human health.

Bioparticles generally refer to the various kinds of microscopic substances in the living body, such as cells, bacteria, viruses, proteins, and nucleic acids. The investigation of their number, function, and structure can characterize information about the health of the individual. For example, virus testing for the genetic material of COVID-19 can determine if the target patient is infected (Reynard et al., 2022). The detection of gut flora can assess a body's metabolic capacity and antibiotic resistance (Patterson et al., 2016). White blood cells (WBCs) are the backbone of the body's immune function, and an increase in WBCs count indicates the severity of the patient's infection (Bain, 2017; Meier et al., 2021). Also, low levels of protein in the body are commonly seen due to liver disease (Lee et al., 2021a), and severe burns (Lang et al., 2019). However, traditional bioparticle detection for medical testing is time-consuming and requires well-equipped facilities, skilled workers, and complex operations (Luppa et al., 2011; Roth-Kleiner et al., 2010). Meanwhile, doctors are not able to provide rapid and effective treatment plans because of the centralised testing process in hospitals. Patients need to commute to the hospital several times during treatment, which increases the burden on both the patient and hospital sides.

To solve these problems, point-of-care testing (POCT) applications

* Corresponding author.
** Corresponding author.
E-mail addresses: guojinhong@cqmu.edu.cn (J. Guo), S.Tang@bham.ac.uk (S.-Y. Tang).

https://doi.org/10.1016/j.bios.2022.114944
Received 8 September 2022; Received in revised form 17 November 2022; Accepted 22 November 2022
Available online 30 November 2022

for bioparticle detection have been proposed in recent years (Gao et al., 2017; Li, 2019; Luppa et al., 2011). POCT is a time-efficient and simple testing method, using portable analytical devices and supporting reagents to detect specific bioparticles. POCT technology brings convenient biomedical diagnosis and proactive health management opportunities for people, particularly in economically underdeveloped countries and regions. Microfluidics integrates processes such as sampling, processing, separation, and detection onto a chip of a few square centimetres. It has the advantages of low reagent consumption, high detection accuracy and short analysis time (Battat et al., 2022; Kumar et al., 2022; Li et al., 2020; Nguyen et al., 2018; Sachdeva et al., 2020). These features perfectly meet the development needs of POCT, making microfluidics the centre of research for the investigation of new generation POCT devices (Gao et al., 2019a; Jung et al., 2015; Zhang et al., 2017a). Moreover, the network of microchannels fabricated in a microfluidic chip enables the control of micron level fluids, thus replacing various functions of conventional biological or chemical laboratories. Compared to a central laboratory, the microfluidic chip-based POCT technology has the following advantages: low consumption of samples to obtain detection results, reduced cost of assay, and decreased possibility of cross-contamination.

A variety of microfluidic platforms have been established to analyse bioparticles (Gong et al., 2018; Tao et al., 2021; Yang et al., 2022). At present, microfluidic bioparticle analysis mainly utilises optical and electrical detection methods (Daguerre et al., 2020; Gong et al., 2018; Li et al., 2018; Stavrakis et al., 2019). Optical detection mainly uses fluorescence (Fan et al., 2018), absorbance (Karakuzu et al., 2021), and image-based methods (Constantinou et al., 2019); these methods have demonstrated outstanding performance in the field of bioparticle detection. However, these optical detection methods require expensive and complex optical components, such as photomultiplier tubes (PMTs) (Hamza et al., 2019), complementary metal–oxide-semiconductor (CMOS) sensors (Heo et al., 2017), photodetector-based imaging devices (Blasi et al., 2016), high speed cameras (Zhang et al., 2017b), field programmable gate arrays (FPGAs) (Sotiropoulou et al., 2014), and laser modules (Chandrasekaran and Packirisamy, 2010), which contribute to the cost and manufacturing complexity of optical detection methods. Thus, using optical detection significantly increases the cost of the POCT devices. Therefore, it is necessary to seek alternative solutions to make the whole platform cost-effective, simple, and miniature. To this end, this review summarises non-optical detection approaches used in microfluidics, including electrical, magnetic, and acoustic methods that possess the potential to be applied in the making of POCT devices. We also briefly summarise methods for manipulating particles that are important for subsequent detection. Each of the detecting methods is described in detail, both in terms of mechanism and typical applications. Finally, a foresight is offered, elucidating underexplored technologies and highlighting the research challenges faced by non-optic-based methods in developing POCT platforms yielding clinical advances.

2. Bioparticle manipulation

Depending on the mechanisms used, methods for microfluidic-based bioparticle manipulation can be divided into passive and active approaches. This section briefly introduces these manipulating techniques, which are important for the selection of subsequent detecting methods.

2.1. Passive methods

2.1.1. Inertia

As cells and particles flow in a microfluidic channel, in addition to being moved forward by the mainstream driving force, they are also influenced by the shear effect lift force (F_{ls}) caused by fluid velocity difference and the wall induced lift force (F_{ws}) caused by channel walls in the vertical direction (Xiang et al., 2014). The combined force of F_{ls} and F_{ws} is often referred to as inertial force. This can be used for manipulating particles (Fig. 1A). The inertial force is affected by many factors such as fluid flow rate, microchannel size, fluid properties, particle shape, volume, and deformation features (Amini et al., 2014).

The advantages of the inertial force approach to microfluidic platforms are: simple design, fast manipulation, high throughput, and high sorting efficiency with minimal damage to the cells.[39] The disadvantage, however, is that inertial force sorting results are highly dependent on the cell sample. A detailed summary of inertia microfluidics for particle manipulation can be found elsewhere (Huang et al., 2020b; Kim et al., 2018; Zhao et al., 2020).

2.1.2. Microfiltration

Microfiltration is considered the most basic passive bioparticle manipulation technique (Fig. 1B). It refers to the use of particle size and deformability to accomplish manipulation. The microfluidic platform can be compatible with geometric structures for microfiltration, such as pores, pillars, weirs, and crossflows (Cheng et al., 2016). By adjusting geometric parameters such as the membrane pore size, the distance between pillars, and the height of weirs, microfiltration based microfluidic chips can block target particles in a particular region based on particles' morphological properties.

The microfiltration method is simple in structure. However, the method is limited by the filtration principle - it is easy to block the microfluidic chips and damage the cells with high pressure. More detailed information on microfiltration for particle manipulation can be found elsewhere (Amar et al., 2019; van Dinther et al., 2013; Zhou et al., 2018).

2.1.3. Deterministic lateral displacement

Deterministic lateral displacement (DLD) is a method which utilises the specific arrangement of arrays of micropillar obstacles within a flat

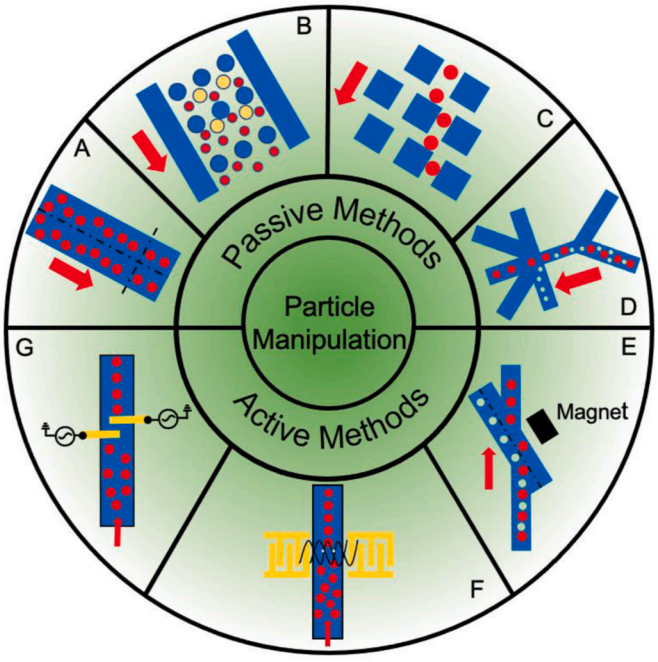

Fig. 1. Schematic of bioparticle manipulation methods, the blue part represents the geometric structure of the chip. (A) Inertia. (B) Microfiltration - only particles smaller than the distance between pillars (red) are permitted to pass through the structure, the others (yellow) will be blocked. (C) Deterministic lateral displacement. (D) Pinched flow fraction - larger particles (red) can travel further towards the centre of the channel than the smaller ones (green) under the effect of the sheath flow, resulting in particle separation. (E) Magnetic - particles (red) with magnetic properties are affected to move into a particular channel. (F) Acoustic. (G) Dielectrophoresis.

microfluidic channel for precisely controlling the trajectory of particles to facilitate their separation (Fig. 1C) (Hochstetter et al., 2020; Xavier et al., 2019). When particles come into contact with pre-set micropillars, particles larger than the critical diameter undergo a lateral movement.

The DLD method exhibits good resolution and high accuracy and has been broadly used in the manipulation of various biological particles from cells to exosomes (Wunsch et al., 2016). Nevertheless, when manipulating particles of many different sizes, it is necessary to redesign the micropillar arrays to obtain the appropriate critical diameter. This reduces the repeatability of the method and increases the cost. More details of the DLD method can be found elsewhere (Murakami et al., 2021; Rezaei et al., 2021; Sherbaz et al., 2022).

2.1.4. Pinched flow fractionation

In a pinched flow fraction (PFF) device, the sheath flow pushes the sample particles to the edge of the microchannel. Larger particles can migrate further towards the centre of the channel than the smaller ones, resulting in particle separation at the outlet of the microfluidic platform (Fig. 1D) (Morijiri et al., 2011). The parameters that influence particle manipulation performance include the flow rate ratio, the pinched section width, and the boundary angle.

The advantages of the PFF method include the simplicity of the chip design and easy operation. However, this method is only available for low concentration samples, and the particles are in contact with the microchannel, which can easily lead to cross contamination and channel blockage. More detailed information about PFF devices can be found elsewhere (Hamacher et al., 2021; Lu and Xuan, 2015; Vig and Kristensen, 2008).

2.2. Active methods

2.2.1. Magnetic manipulation

The manipulation of bioparticles *via* magnetic fields has several applications in practical clinical medicine. Magnetic based bioparticle manipulation can be classified into two categories according to the type of magnet used, electromagnet or permanent magnet (Hejazian et al., 2015). Electromagnets can provide a controllable magnetic field, but the Joule heating effect at high currents may have an impact on the biological reaction of some particles. Given these limitations, it is preferable in most studies to place permanent magnets on the side of microfluidic platforms for magnetic actuation (Fig. 1E).

Magnetic manipulation in microfluidic platforms has several advantages. The magnetic force generally does not influence biological activity in samples; also, the magnetic force does not affect the external media environment and the magnet is not in direct contact with the fluid. However, the magnetic manipulation method needs an additional preparation process to label the target particles with immunomagnetic beads, which increases the operation time and complexity. More detailed information on the magnetic method for particle manipulation can be found elsewhere (Alnaimat et al., 2018; Luo and He, 2020; Yaman et al., 2018).

2.2.2. Acoustic manipulation

Acoustic waves can be applied directly to bioparticles to control their movements (Fig. 1F). To realise acoustic based manipulation, standing or travelling waves need to be generated. Acoustic forces guide particles, allowing them to concentrate or separate based on their physical properties (Zhang et al., 2020). There are two forms of acoustic waves used in microfluidics - bulk acoustic waves (BAWs) and surface acoustic waves (SAWs). BAWs are longitudinal or shear waves that propagate through the bulk of the microfluidic substrate or channel chamber. In a BAW device, piezoelectric transducers are fixed under or on the side of the microfluidic channel and BAWs are coupled to the channel that is made of high acoustic impedance materials to form an acoustic resonator (Lenshof et al., 2012). Unlike BAWs, SAWs propagate along the surface of the substrate material. In a SAW microfluidic device, SAWs are generated by interdigitated transducers (IDTs) formed by depositing comb-like electrodes on a piezoelectric crystal such as lithium niobate ($LiNbO_3$) (Ozcelik et al., 2022). The interference of acoustic waves in BAW/SAW devices results in standing acoustic wave fields that can form pressure nodes and pressure antinodes for particle manipulations.

Acoustic waves can control particles on a microscale with high efficiency and low invasiveness. However, the size and the number of particles that can be manipulated by acoustic methods are determined by the wavelength of the acoustic waves; and in order to control smaller particles, microfluidic platforms need to be equipped with acoustic generators of higher frequency and power. More details of acoustic manipulation of particles can be found elsewhere (Chen et al., 2021; De Stefano et al., 2022; Gao et al., 2020).

2.2.3. Dielectrophoretic manipulation

Dielectrophoresis (DEP) is a phenomenon of relative movements of particles and other dielectrics in a non-uniform electric field due to the force of polarization (Fig. 1G) (Cetin and Li, 2011). The magnitude of the dielectric force is not only determined by the size and the electrical property of the particles, but it is also influenced by the frequency of the applied electric field. The DEP force exerted on a particle is generated from the interaction between the nonuniform electric field and the induced dipole moment within the particle (Khoshmanesh et al., 2011; Morgan and Green, 2003; Tang et al., 2013). Depending on the dielectric properties of the particle and the surrounding medium, as well as the frequency of the applied AC electric field, the particle motion can be directed either toward (positive DEP or pDEP) or away from (negative DEP or nDEP) regions of high electric field intensity.

Bioparticle manipulation using the DEP method can be achieved using low voltages and does not require any labelling steps, which is promising for instrumentation and miniaturisation. However, the complexity and high cost of electrode fabrication, as well as the negative impact of the electric field on bioparticles, are the main factors that limit the development of DEP manipulation. More detailed information on DEP manipulation can be found elsewhere (Huang et al., 2018; Ramirez-Murillo et al., 2021; Zhang et al., 2019a).

3. Bioparticle detection using non-optical platforms

After the sorting and focusing process, numerous non-optical microfluidic platforms based on electrical, magnetic, and acoustic techniques can be used for the detection and characterisation of bioparticles, as summarised in Table 1. The following sections will elucidate the principle of each technique and discuss microfluidic detection platforms leveraging these techniques.

3.1. Electrical methods

3.1.1. Mechanisms

Electrical methods for detection and characterisation are based on measuring the impedance of bioparticles activated by an AC or DC signal in a medium. When using an AC voltage $\widetilde{U}$ with a specific frequency as the excitation signal, and the current response of the detection platform is $\widetilde{I}$, the electrical impedance of the bioparticle can be determined as.

$$\widetilde{Z} = \frac{\widetilde{U}}{\widetilde{I}} \tag{1}$$

Most works use Maxwell Mixture Theory (MMT) (Nasir and Al Ahmad, 2020) and the Equivalent Circuit Model (ECM) (Berli, 2007) to interpret the impedance information of bioparticles in a suspension. In general, the electrical properties of different parts of a cell are not identical, so modelling of the shell (membrane and cell wall) and the cytoplasm is required to estimate the complex permittivity of a cell. For a mammalian cell, the sphere model consists of a conducting sphere (cytoplasm) and an insulating thin shell (cell membrane) (Cheung et al.,

Table 1
Summary of non-optical microfluidic-based platforms for bioparticle detection.

Category	Detection Method	Remarks	Throughput	Limit of Detection	Ref.
RBCs and WBCs	Impedance analysis	Coulter counter	Over 3000 cells per s	0.0025 cells per pL	(Chun et al., 2005)
Yeast cells	Impedance analysis	Coulter counter	1000 particles per s	–	Rodriguez-Trujillo et al. (2008)
RBCs	DC impedance analysis	Coulter counter	1800 particles per min	–	Zhang et al. (2019b)
F. tularensis	DC impedance analysis	Coulter counter	–	–	Choi et al. (2014)
Murine breast cancer cells	DC impedance analysis	MOSFET-based Coulter counter	2.37 cells per s	3×10^7 cells per mL	Sun et al. (2012)
CRP, NT-proBNP, cTnI, and fibrinogen	DC analysis	FET sensor arrays	–	CRP: 0.14 mg/L; NT-proBNP: 0.832 pg/mL; cTnI: 0.394 pg/mL; fibrinogen: 20.2 mg/dL	Sinha et al. (2019)
Human polymorphonuclear leukocytes and fish RBCs	AC impedance analysis	Coplanar electrodes (100 Hz–2 MHz)	–	–	(Ayliffe and Rabbitt, 1999)
RBCs	AC impedance analysis	Coplanar electrodes (100 kHz–15 MHz)	100 cells per s	–	Gawad et al. (2001)
RBCs	AC impedance analysis	Coplanar electrodes (400 kHz–800 kHz)	–	4×10^6 cells per mL	Mahesh et al. (2020)
DNA	AC impedance analysis	DEP based counting	–	–	
IL-6	AC impedance analysis	Coplanar electrodes (700 kHz)	–	50 pM	Mok et al. (2014)
Yeast cells	AC impedance analysis	Coplanar electrodes	~3 to 6 cells per s	~107 cells per mL	Xie et al. (2019)
Euglena gracilis	AC impedance analysis	Coplanar electrodes	–	–	Tang et al. (2021)
C. elegans worms	AC impedance analysis	Coplanar electrodes (300 kHz)	~30 worms per minute	–	Zhu et al. (2018)
RBCs	AC impedance analysis	Coplanar electrodes (0.1 MHz–10 MHz)	7200 cells per s	–	Panwar and Roy (2019)
RBCs	AC impedance analysis	Coplanar electrodes (500 kHz)	–	–	Yang and Ai (2019)
RBCs	AC impedance analysis	Facing electrodes (350 kHz–20 MHz)	1000 cells per minute	–	Cheung et al. (2005)
Yeast cells	AC impedance analysis	Facing electrodes (0.5 MHz–250 MHz)	–	5×10^6 to 10×10^6 cells per mL	Haandbaek et al. (2014a)
E.colis and *B.subtilis*	AC impedance analysis	Facing electrodes (80 MHz–200 MHz)	–	1×10^6 cells per mL	Haandbaek et al. (2014b)
Gram-negative bacterial cell	AC impedance analysis	Facing electrodes (5 MHz–40 MHz)	1000 cells per s	–	Spencer et al. (2020)
Yeast cells	AC impedance analysis	Facing electrodes (100 kHz–5 MHz)	–	10^2 cfu per mL	Mansor et al. (2017)
RBC and yeast cells	AC impedance analysis	Facing electrodes (615 kHz and 500 kHz)	2500 cells per s	–	Honrado et al. (2020)
Pancreatic cancer cells	AC impedance analysis	Facing electrodes (0.5 MHz–30 MHz)	–	–	Honrado et al. (2022)
Human ovarian, breast, and prostate cancer cells	AC impedance analysis	Coulter counter (460 kHz)	–	–	Wang et al. (2019)
Pancreatic cancer cells	Giant magnetoresistance (GMR)	–	2730 cells per minute	–	Huang et al. (2020a)
RBCs	GMR	–	10,000 cells per s	–	Reisbeck et al. (2016)
Colon adenocarcinoma cells	GMR	–	–	2.66 cells per μL	Chicharo et al. (2018)
FP, CEA, CYFRA21-1, NSE, SCC, PG I, PG II, CA19-9, total PSA, free PSA, free-β-hCG, Tg	GMR	–	–	FP: 0.52 ng/mL; CEA: 0.27 ng/mL; CYFRA21-1: 0.25 ng/mL; NSE: 0.5 ng/mL; SCC: 0.3 ng/mL; PG I: 1 ng/mL; PG II: 0.5 ng/mL; CA19-9: 2 u/mL; total PSA: 0.02 ng/mL; free PSA: 0.07 ng/mL; free-β-hCG: 0.3 ng/mL; Tg: 1 ng/mL	Gao et al. (2019b)
Prostate specific antigen (PSA)	Giant magnetoimpedance (GMI)	–	–	0.1 ng per mL	Feng et al. (2019)
Human IgG	QCM	–	–	0.1 ng/mL	Han et al. (2011)

(*continued on next page*)

Table 1 (*continued*)

Category	Detection Method	Remarks	Throughput	Limit of Detection	Ref.
Cancer cells	Acoustic radiation	–	–	–	Hartono et al. (2011)
Human alveolar basal epithelial, human airway smooth muscle, and breast cancer cells	SAW	–	–	–	Wu et al. (2019)
MDA MB231 cells	SAW	–	~10 cells per second	–	Wu et al. (2021)
CRP	SAW	–	–	4 ng/mL	Jeng et al. (2021).
Acute myeloid leukemia cells and HT29 colorectal cancer cells	Ultrasound scattering signal	375 MHz	–	5×10^6 cells per mL	Strohm et al. (2019)
RBCs and WBCs	Ultrasound backscatter and photoacoustic	375 MHz	150 cells per min	–	Gnyawali et al. (2019)

2010). At low frequencies, the cell has a large permittivity and a small electrical conductivity, showing high insulation and low conductivity, and impedance amplitude predicts the size of the cell. As the frequency gradually increases, the capacitance of the cell membrane and the permittivity of the cell decrease, but the conductivity gradually increases, and the impedance signal provides information about membrane properties. With further increase of frequency, the high frequency electric field can apply to the cell interior and the cell exhibits low insulation and high conductivity, and the impedance information provides information about the cell interior. The complex permittivity of the cell ($\widetilde{\varepsilon}_p$) is a function of cell membrane complex permittivity ($\widetilde{\varepsilon}_{mem}$), cytoplasmic complex permittivity ($\widetilde{\varepsilon}_i$), and cell radius ($R$), which can be expressed as:

$$\widetilde{\varepsilon}_p = \widetilde{\varepsilon}_{mem} \frac{\gamma^3 + 2\frac{\widetilde{\varepsilon}_i - \widetilde{\varepsilon}_{mem}}{\widetilde{\varepsilon}_i + 2\widetilde{\varepsilon}_{mem}}}{\gamma^3 - 2\frac{\widetilde{\varepsilon}_i - \widetilde{\varepsilon}_{mem}}{\widetilde{\varepsilon}_i + 2\widetilde{\varepsilon}_{mem}}} \tag{2}$$

where $\gamma = (R + d)/R$, and d is the thickness of the cell membrane.

When the volume fraction of cells in solution is small, the complex permittivity of the single-cell suspension system ($\widetilde{\varepsilon}_{mix}$) can be calculated as:

$$\widetilde{\varepsilon}_{mix} = \widetilde{\varepsilon}_m \frac{1 + 2\Phi\widetilde{f}_{CM}}{1 - \Phi\widetilde{f}_{CM}} \tag{3}$$

where Φ is the volume fraction, $\widetilde{\varepsilon}_m$ is the complex permittivity of the suspension medium, and $\widetilde{f}_{CM}$ is the Clausius-Mossotti factor, which is expressed as:

$$\widetilde{f}_{CM} = \frac{\widetilde{\varepsilon}_p - \widetilde{\varepsilon}_m}{\widetilde{\varepsilon}_p + 2\widetilde{\varepsilon}_m} \tag{4}$$

The electrical impedance ($\widetilde{Z}_{mix}$) of a single-cell system can be calculated according to the following equation:

$$\widetilde{Z}_{mix} = \frac{1}{j\omega\widetilde{\varepsilon}_{mix}G_f} \tag{5}$$

where $j^2 = -1$, $\omega = 2\pi f$ is the angular frequency and G_f is a constant of the detection area. For an ideal two parallel plate electrode system, G_f is calculated as S/w, where S is the surface area of the electrodes and w is the distance between the two electrodes.

The ECM describes the electrical properties of a cell in the impedance detection area after modelling them into equivalent circuits. When a DC electric field is applied to the detection area, bioparticles can be regarded as homogeneous insulating spherical particles and the intensity of the resulting signal is related to the ratio of the particle size to the channel (detection aperture) dimension. When an AC electrical field is applied to the detection area, circuit modelling can be used to obtain the characteristic parameters of the bioparticle.

Electrical methods can be categorised depending on the current applied to the electrodes, in the following sections, we summarise the recent applications using DC or AC based impedance analysis methods.

The DC sensing circuit is simple in design and requires fewer peripherals, but the DC current may degrade electrodes due to electrochemical reactions, causing variations in signal detection. On the other hand, the AC method suppresses electrochemical reactions but requires peripheral instrumentations for signal generation and processing, which increases the complexity of the sensing circuit. However, the AC method effectively enables the characterisation of the internal properties of bioparticles using different frequencies.

3.1.2. Detection methods based on DC impedance analysis

A Coulter counter is an effective and automated method for enumerating and investigating single cells (Song et al., 2017). As shown in Fig. 2A, the principle used is to measure the change of electrical impedance under a DC voltage as bioparticles flow through a circular channel (aperture) (Yan et al., 2022). The counter records the current pulses caused by each particle passing through the sensing region, and the number and peak value of current pulses correspond to the number and volume information of the detected particles.

Larsen proposed the first miniaturised Coulter counter (MCC) by machining a detection aperture and microfluidic channels on a single-crystal silicon substrate and placing a four-electrode measuring system inside the flow channel (Larsen and Branebjerg, 1997). However, no particle counting related data was obtained in this study. The choice of electrode material is a critical issue when fabricating MCCs - appropriate electrodes can not only work for a long time, but can also be easily integrated into the microfluidic chip. The contact interface between the metal electrodes and the suspension tends to form an electrical double layer (EDL), which greatly reduces the performance of the counter. To solve the problem, salt bridge electrodes have been used to eliminate EDL. As shown in Fig. 2B, Chun used polyelectrolyte gel filled with isotonic NaCl solution for detection, and the gel was connected to a DC impedance analyser via Ag/AgCl electrodes to form a measurement circuit (Chun et al., 2005). This platform successfully discriminated red blood cells (RBCs) and WBCs and reached a detection throughput of 1000 cells/s.

The size of the detection aperture determines the size of the particle that can be detected in an MCC. To enable the detection of particles with a large size range, Rodriguez et al. reported a differential impedance detection MCC which is capable of adjusting the sensing aperture (Rodriguez-Trujillo et al., 2008). Particles with diameters between 5 and 20 μm can be detected using the MCC. However, the mechanically adjustable sensing aperture increases the assay time and operation complexity. To solve this problem, Zhang et al. connected multiple sensing apertures in series to achieve the same ability to sense particles with various sizes in a MCC (Fig. 2C) (Zhang et al., 2019b). In this study, the detection circuit generates multiple time-related resistive pulse signals as particles pass through the sensing aperture array. The overall signal-to-noise ratio was improved by applying multiple cross-correlation analysis.

Reducing the aperture size in pursuit of a smaller sensing area to improve sensitivity and accuracy may result in mechanical blockage and counter breakdown. To solve this problem, Kim and Kim used

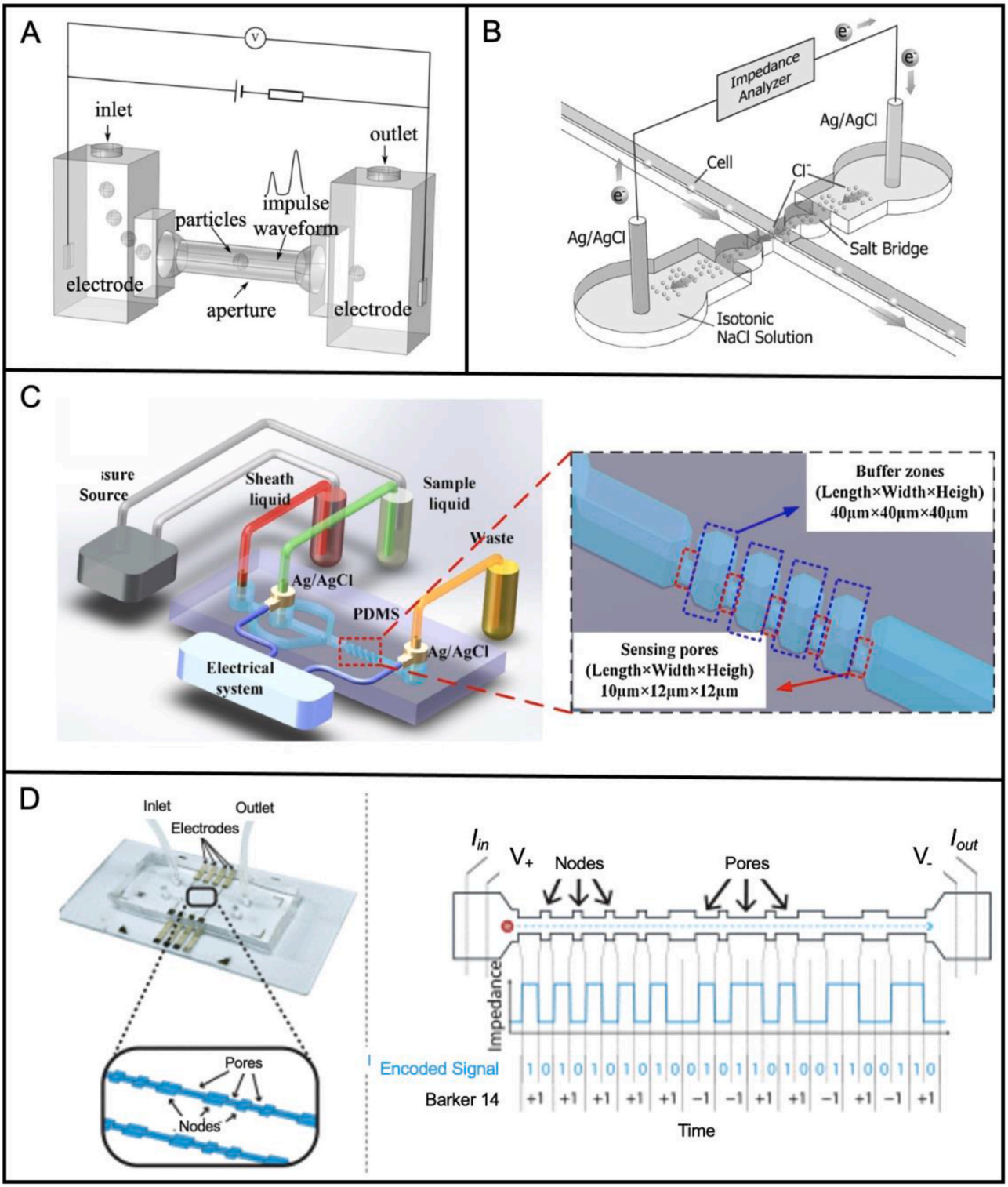

Fig. 2. Microfluidic MCC platforms. (A) Schematic and working principle of a Coulter counter. Reproduced with permission (Yan et al., 2022). Copyright 2020, Royal Society of Chemistry. (B) Schematic of the Coulter detection platform based on a polyelectrolyte salt bridge. Reproduced with permission (Chun et al., 2005). Copyright 2005, American Chemical Society. (C) Schematic of a Coulter detection platform based on a multiple sensing apertures structure. Reproduced with permission (Zhang et al., 2019b). Copyright 2019, Elsevier. (D) Schematic of a Coulter detection platform based on binary code. Reproduced with permission (Kellman et al., 2018). Copyright 2018, IEEE.

pneumatically actuated elastomeric valves to effectively eliminate mechanical blockages (Kim and Kim, 2013); however, this method adds complexity to the instrument, making this solution difficult to be used in commercial devices. To reduce the complexity of the device, Choi et al. set a pair of polyelectrolyte gel electrodes on the same side of the flow channel and introduced a non-conducting sheath fluid on the other side of the channel to act as a movable virtual wall (Choi et al., 2014). The flexible adjustment of the effective aperture is achieved by controlling the flow rate of the sheath fluid, and the size distribution of submicron-scale bacteria was successfully characterised.

The simplicity of the MCC also allows the use of simple electronic components to improve detection performance. Sun et al. used a metal–oxide–semiconductor field-effect transistor (MOSFET) in a MCC and combined it with a DEP sorter to achieve on-chip cell separation and quantitative characterisation (Sun et al., 2012). The movement of cells within the sensing channel causes a change in the MOSFET gate potential, which can be amplified by the change of the MOSFET's drain current. The magnitude of the current change is related to the cell volume. The use of a MOSFET makes the chip structure and system composition simpler, thus lowering the manufacturing threshold for MCCs. Moreover, detection platforms equipped with field effect transistors (FETs) enable fast, reliable, and sensitive protein sensing functions. For example, Sinha et al. developed an integrated microfluidic platform for the detection of cardiovascular disease protein biomarkers by immobilising specific aptamer probes on FET sensor arrays (Sinha et al., 2019). This system allows rapid (5 min) analysis of four biomarkers of cardiovascular disease, i.e., C-reactive protein (CRP), N-terminal pro b-type natriuretic peptide (NT-proBNP), cardiac troponin I (cTnI), and fibrinogen from clinical samples (~4 μL).

In addition to optimising hardware components, some researchers have explored the use of efficient signal processing and data analysis algorithms to improve the performance of the platform. As shown in Fig. 2D, Kellman et al. simulated the microfluidic channel as a communication system, modulating the response amplitude of particles by means of nodes and pores in the channel, allowing the particles to be encoded like packets of data (Kellman et al., 2018). In this way, the entire platform can be used to detect and separate target particles using signal processing methods.

3.1.3. Detection methods based on AC impedance analysis

DC impedance-based microfluidic platform detection technology has greatly expanded the ability to analyse bioparticles. However, in order to avoid electrochemical reactions between electrodes and to further analyse the internal electrical properties of cells, numerous works have been conducted studies on AC-based microfluidic impedance cytometry (MIC) in the past decades.

Ayliff proposed the world's first single-cell continuous AC impedance analysis platform. The platform has microchannels on a glass substrate and a pair of gold plated electrodes on either side of the narrowest part of the channel (Ayliffe and Rabbitt, 1999). By calculating impedance within a range of frequencies from 100 Hz to 2 MHz, the platform can distinguish human polymorphonuclear leukocytes and fish RBCs. Based on this work, researchers have made significant progress in the continuous AC impedance detection of single cells on microfluidic chips. One important development is a platform with a coplanar electrode structure, as proposed by Gawad et al., (2001). As shown in Fig. 3A, three electrodes are placed side by side on the same surface of the microfluidic channel. The adjacent two groups of electrodes compose two sensing zones (Z_{AC} and Z_{BC}), which are used to differentially measure impedance signals. The device allowed screening rates of over 100 samples/s with frequencies ranging from 100 kHz to 15 MHz. In order to extend AC impedance analysis to the lower frequency range, Zheng et al. performed black platinum plating on the coplanar electrode surface (Zheng et al., 2008). The platinum black electrodes have high surface roughness, which effectively eliminates the influence caused by the EDL induced capacitance and improves the detection capability in the intermediate frequency range (~100 Hz to 7 MHz). Additionally, Mahesh et al. observed a unique reactive current that occurs only at the low frequency interval (400–800 kHz) in MIC with coplanar electrodes and defined it as the double peak phenomenon (Mahesh et al., 2020). The high sensitivity of the double peak in response to changes in cell membrane capacitance was used to detect the dielectric properties of normal and glutaraldehyde treated erythrocytes. The use of two pairs of electrodes and the double peak phenomenon allows the system to perform cell size and membrane capacitance measurements at a single frequency, thus significantly reducing associated electronic elements (Fig. 3B). Cottet et al. investigated the effect of geometrical parameters of coplanar electrode configurations on the sensitivity of MIC using numerical simulations in combination with experiments (Fig. 3C) (Cottet et al., 2019). This investigation demonstrated that reduced distance between electrodes can improve the sensitivity of the device. Another interesting study uses DEP to detect DNA in a simple microfluidic platform (Nakano et al., 2019). During the detection process, after the target DNA is attached to particles with nDEP properties, the surface conductivity of the particles increases due to the binding of charged DNA molecules. Once a certain amount of DNA is bonded, the DEP changes from negative to positive. Therefore, only the DNA-labelled particles can be attracted to the electrodes by pDEP force, and the captured particles can be counted by impedance measurements. Mok et al. proposed a digital microfluidic platform with a dual chamber structure, in which the capture/reaction chamber has fixed probe molecules for capturing target antigens, while the other chamber is for electrical impedance sensing (Mok et al., 2014). By counting the eluted beads from the capture/reaction chamber using the electrical impedance sensor located in the other chamber, this work demonstrates the detection of the human cytokine interleukin 6 (IL-6) with a higher sensitivity than the traditional enzyme-linked immunosorbent assay (ELISA) method.

The shape of a bioparticle can vary from simple spherical to more complex rod-like or even irregular. Xie et al. used a MIC platform to distinguish spherical and rod-shaped particles with similar volumes/lengths (Xie et al., 2019). As shown in Fig. 3D, rod-shaped cells take longer to travel through the detection area than spherical cells, this results in different widths, amplitudes, and amplitude to width ratios of the impedance signal. Furthermore, the same technique can be used to analyse large biological samples, even though they possess high motility, variable morphology, and a wide range of sizes. Tang et al. developed a MIC platform and a new approach for measuring the shape of single cells/particles (Fig. 3E) (Tang et al., 2021). This work shows that impedance signal data for irregularly shaped objects has a tilt. The amount of tilt is related to the asymmetry level of a particle and is independent of its' trajectory. Zhu et al. used a similar configuration to detect the *Caenorhabditis elegans* (*C. elegans*) worm (Zhu et al., 2018). During impedance signal processing, a kernel density estimation approach was used to analyse worm length-related values for identifying their developmental stages.

Conventional impedance microfluidic devices require professional microfabrication facilities (e.g., metal sputtering or vapor deposition) for generating metal electrodes, which limits the application of these devices to a wider range of fields. To make the fabrication process simpler, Panwar and Roy fabricated compatible coplanar electrodes in a multilayer elastomeric element with Field's metal using one single photolithography step, and the electrodes showed superior measurement performance compared to platinum electrodes for single RBC detection (Panwar and Roy, 2019).

For impedance-based cell detection, the position of the cell/particle travelling inside the microchannel affects the signal, meaning even identical cells/particles travelling along different trajectories can generate different signals. To solve this problem, Brazey et al. developed a star-shaped electrode to mitigate the dependence of the cell position (Fig. 4A) (Brazey et al., 2018). A continuous waveform can be obtained for the star-shaped electrode configuration, while the conventional square-shape electrodes give a saturated signal. Such continuous signals provide an opportunity to recover the trajectory of the detected object, thereby mitigating the dependence on precise control of particle position. In addition, As shown in Fig. 4B, Wang et al. presented a pair of non-parallel electrodes to form a V pattern to detect the position of particles flowing in the channel (Wang et al., 2017). The V-shaped electrodes bring a gradually changing electric field inside of the channel, so particles in different positions experience different electric field strengths and travelling times, thereby showing different impedance results. Similarly, Yang and Ai presented a MIC platform based on N-shaped electrodes for measuring the lateral position of individual cells

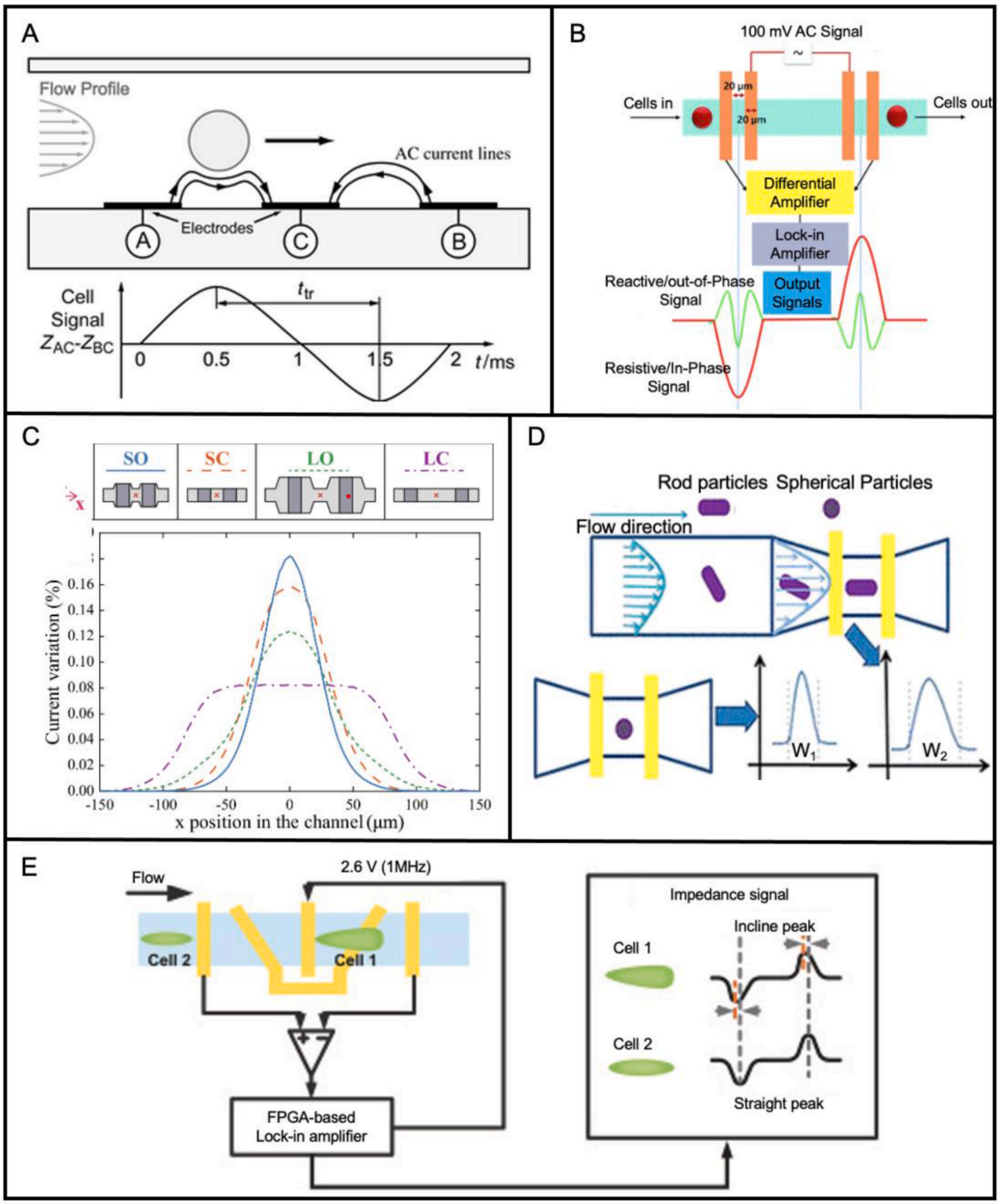

Fig. 3. MIC platforms with coplanar electrode structures. (A) Schematic of a coplanar electrode structure. Reproduced with permission (Gawad et al., 2001). Copyright 2001, Royal Society of Chemistry. (B) Schematic of the double peak behaviour based coplanar electrode impedance microfluidic platform. Reproduced with permission (Mahesh et al., 2020). Copyright 2020, Royal Society of Chemistry. (C) Schematic of an impedance microfluidic platform with four coplanar electrode designs. Four configurations including short optimised (SO), short conventional (SC), long optimised (LO) and long conventional (LC) are tested. Reproduced with permission (Cottet et al., 2019). Copyright 2019, Springer Nature. (D) Schematic of an impedance microfluidic platform that can distinguish particle shapes. Reproduced with permission (Xie et al., 2019). Copyright 2019, American Chemical Society. (E) Schematic of a tilt measurement-based impedance microfluidic platform. Reproduced with permission (Tang et al., 2021). Copyright 2021, Elsevier.

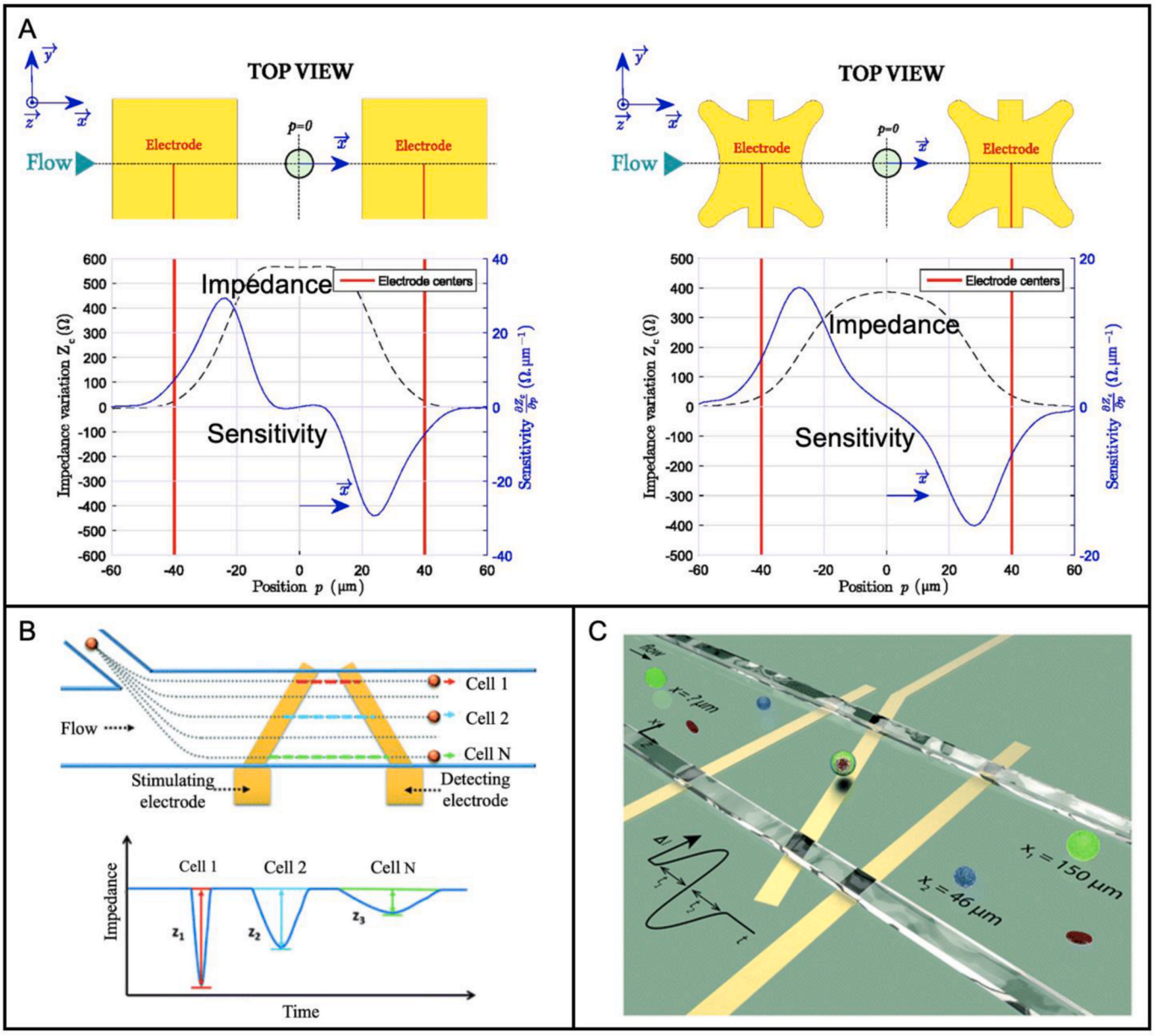

Fig. 4. Methods to eliminate position dependence in coplanar electrode structure MIC platforms. (A) Schematic of square and star shaped coplanar electrode and impedance signal variations. Reproduced with permission (Brazey et al., 2018). Copyright 2018, Royal Society of Chemistry. (B) Schematic of a V-shaped coplanar electrode impedance microfluidic platform. Reproduced with permission (Wang et al., 2017). Copyright 2017, Royal Society of Chemistry. (C) Schematic of an N-shaped coplanar electrode impedance microfluidic platform. Reproduced with permission (Yang and Ai, 2019). Copyright 2019, Royal Society of Chemistry.

or particles (Yang and Ai, 2019). As shown in Fig. 4C, an AC voltage (3 V, 500 kHz) is applied to the tilted electrode and the differential signal is measured from the other pair of electrodes. Due to the asymmetry of the N-shaped configuration, the time and current signal variation of the detected bioparticles passing through the sensing region at different positions are different, which not only determines the lateral position of the particles in the detection area, but also allows their physical properties to be investigated.

A major problem associated with coplanar electrode structure is that all electrodes are placed at the bottom of the flow channel, which generates nonhomogeneous electric field distribution in the sensing area and leads to compromised signal stability. To solve this problem, Cheung et al. placed electrodes on two opposite walls facing each other (facing electrode configuration), as shown in Fig. 5A (Cheung et al., 2005). Compared with coplanar electrodes, the electric field distribution of the facing electrode configuration is more symmetrical and uniform, as shown in the simulation results obtained by Daguerre et al. (Fig. 5B) (Daguerre et al., 2020). The maximum impedance variation can be obtained when a particle is located exactly in the centre between the two electrodes. Using a similar electrode configuration, Haandbaek et al. incorporated a series resonant LC circuit into an impedance measurement circuit to enhance the impedance phase shift when cells flow through a microfluidic channel, thereby improving the detection sensitivity (Haandbaek et al., 2014a). In this study, the cells/particles first pass through the DEP focusing electrodes to minimise the influence of position before entering the detection electrodes. The device used a high-frequency lock-in amplifier that can measure the AC impedance up to 500 MHz to investigate the internal dielectric properties of cells (Haandbaek et al., 2014b). The high frequency capability of the device makes it possible to distinguish wild-type yeast cells from a mutant strain. Antimicrobial resistance is a very challenging problem and Spencer et al. proposed a simple and rapid platform for antimicrobial

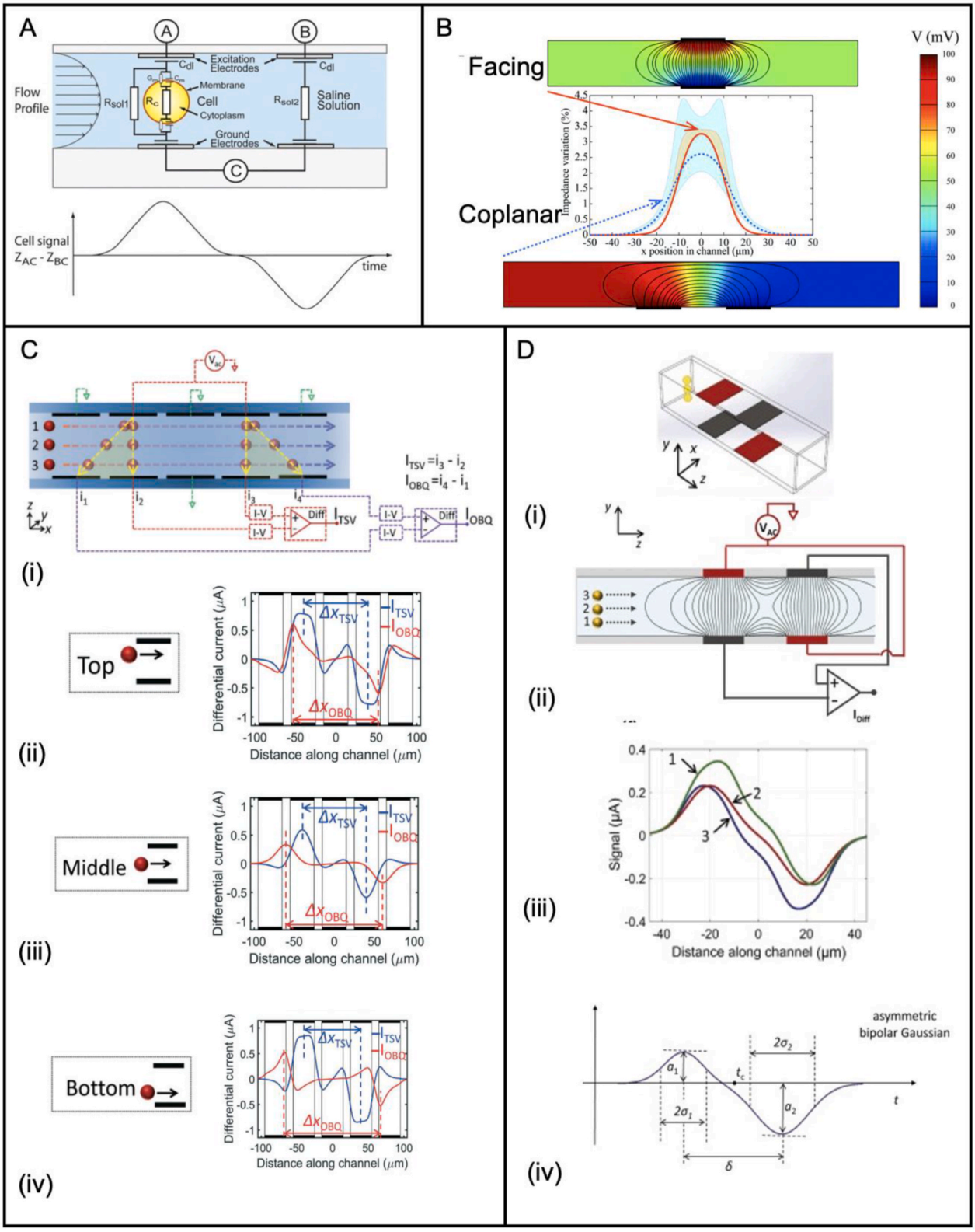

Fig. 5. MIC platforms with a facing electrode structure. (A) Schematic of a facing electrode structure. Reproduced with permission (Cheung et al., 2005), Copyright 2005, John Wiley and Sons. (B) Schematic of the electric field distribution for coplanar electrodes and facing electrodes. Reproduced with permission (Daguerre et al., 2020). Copyright 2020, Royal Society of Chemistry. (C) Schematic of five pairs of facing electrode structure (i) Side view of a facing electrode configuration array with multiple electrode pairs. Resulting signals from three different movement trajectories, top (ii), middle (iii), and bottom (iv). Reproduced with permission (Spencer et al., 2016). Copyright 2016, Royal Society of Chemistry. (D) Schematic of facing electrodes with opposite electric field directions (i) 3D view and (ii) side view of the wiring format. (iii) Signal waveforms of three different movement trajectories (top, middle, and bottom). (iv) A particle passing through the sensing region generates two half waves with different amplitudes and widths. Reproduced with permission (Caselli et al., 2018). Copyright 2018, Elsevier.

susceptibility testing (Spencer et al., 2020). The MIC with facing electrode configuration can measure approximately 10^5 cells within a time window of 2–3 min to determine the response curve.

Despite the fact that the facing electrode configuration largely eliminates the influence of an inhomogeneous electric field, the intensity of the electric field close to the electrodes still differs from that in the central region, and thus there remains some position dependence. Instead of finding strategies to eliminate the dependence of particle position, an alternative approach is to precisely extract the information about particle position using more complex electrode configurations. Spencer et al. built a facing electrode configuration array with multiple electrode pairs to characterise cells/particles with high accuracy (Spencer et al., 2016). As shown in Fig. 5C(i), four electrodes are grounded and the remaining two electrodes at the top are connected to an AC signal generator. Together with operational amplifiers, the four bottom detection electrodes can generate two differential signals in both transverse (TSV) and oblique (OBQ) directions. By calculating the peak-to-peak ratio of the TSV and OBQ current signals, it was found that the value only depends on the transversal position (i.e., Top, Middle, or Bottom shown in Fig. 5C(ii)-(iv)) of cells/particles in the channel. To further extract the lateral position information of a particle in the channel, Caselli et al. used two pairs of electrodes and applied an AC voltage to diagonally opposite electrodes (Fig. 5D(i)-(ii)) (Caselli et al., 2018). A particle moving in the upper half of the channel (Fig. 5D(ii-iii), trajectory 3) is located closer to the top electrode in both the upstream and downstream sensing regions. This results in unequal amplitudes and widths of the half-wave generated by one particle in these two sensing regions (Fig. 5D(iv)). Such a difference can be used to provide information on particle position in the channel.

The above-mentioned MIC platforms mainly use embedded

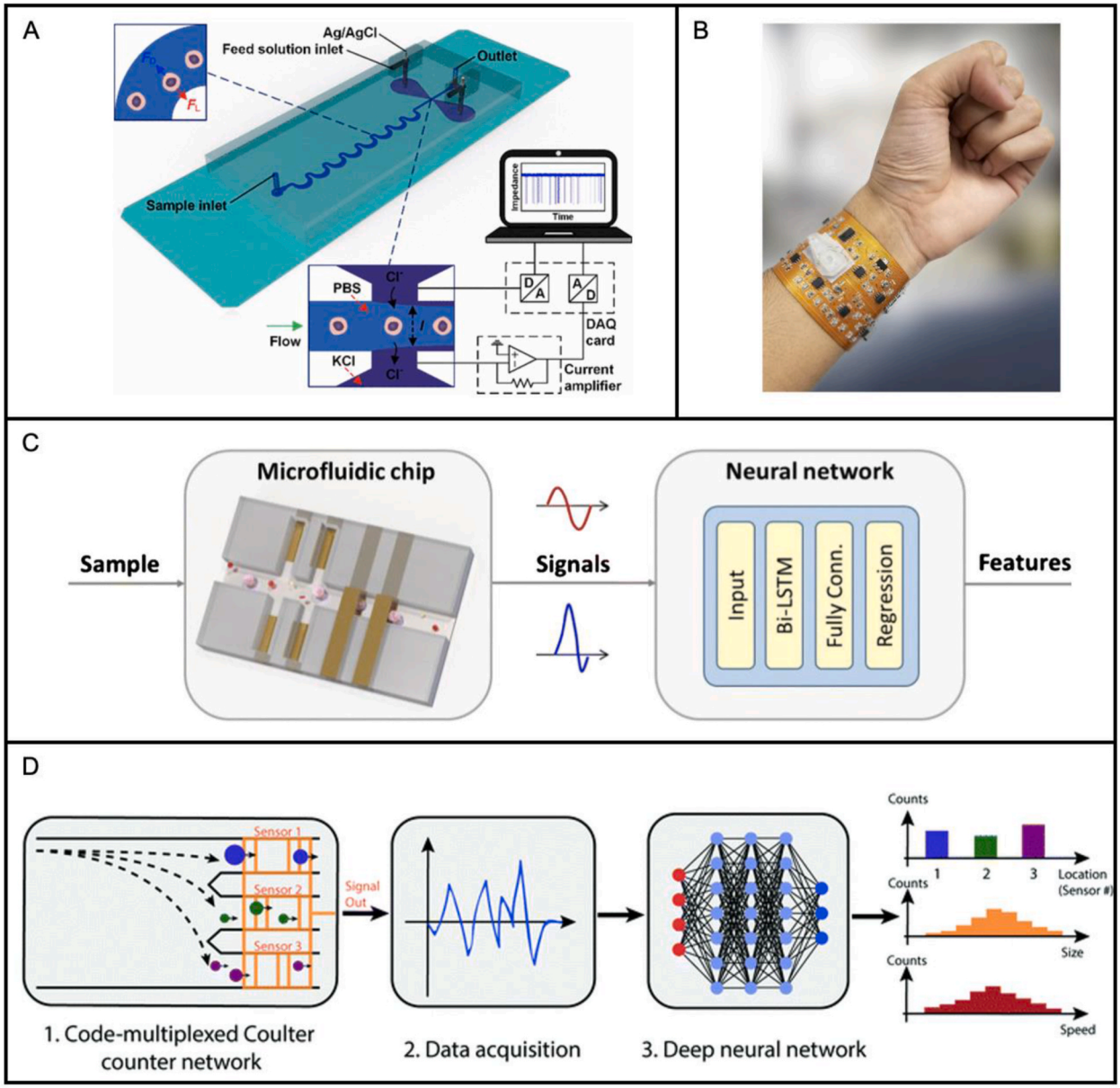

Fig. 6. Emerging microfluidic impedance analysis platforms. (A) Schematic and working principle of a liquid electrode MIC platform. Reproduced with permission (Tang et al., 2017). Copyright 2017, American Chemical Society. (B) Schematic of a wearable impedance microfluidic platform on a flexible circuit board. Reproduced with permission (Furniturewalla et al., 2018). Copyright 2018, Springer Nature. (C) Schematic of a neural network-based impedance microfluidic chip. Each current signal is used as a cell fingerprint and fed into the neural network for real-time feature extraction. Reproduced with permission (Honrado et al., 2020). Copyright 2020, Springer Nature. (D) Schematic of a neural network-based Coulter microfluidic platform. Each current signal is generated by a microfluidic sensor network and processed through a neural network. Reproduced with permission (Wang et al., 2019). Copyright 2019, Royal Society of Chemistry.

electrodes for measurements, which require rather expensive and complicated electrode manufacturing processes. Besides, it is also a great challenge to clean embedded electrodes for reusing. Mansor et al. attempted to solve this problem by using two tungsten needles instead of microfabricated electrodes for cell detection (Mansor et al., 2017). The microneedles can be easily removed from the microchannel for reusing after ultrasonic cleaning. Solid electrodes often require a complicated assembly process, whereas some studies use conductive liquids as detection electrodes with a simpler fabrication process. As shown in Fig. 6A, Tang et al. inserted Ag/AgCl wires into a chamber containing liquid electrodes for cell counting and discrimination. Innovative materials can even make the MIC flexible and wearable (Tang et al., 2017). For example, as shown in Fig. 6B, Furniturewalla et al. proposed a wearable MIC blood cell count analyser which is integrated into a flexible circuit wristband (Furniturewalla et al., 2018). The wristband consists of a lock-in amplifier, an analogue-to-digital converter (ADC), and a wireless Bluetooth module for realising real-time smartphone readings.

Intelligent microfluidics takes advantage of the powerful data processing capabilities of machine learning (ML) to improve the performance of systems to analyse biological samples (Zheng et al., 2021). Following this trend, MIC systems also adopted ML for analysing single cells. For instance, Honrado et al. designed a recurrent neural network to process the signals provided by a MIC chip for enabling real-time multi-parameter analysis of impedance signals (Fig. 6C) (Honrado et al., 2020). The deep learning model is capable of accurately characterising the volume, velocity, and cross-sectional position (lateral and vertical) of particles and cells. Furthermore, they also found that pancreatic cancer cells have different AC responses when they are in viable, early apoptotic, late apoptotic, and necrotic states. When combined with unsupervised learning clustering and supervised learning classification, the whole platform is able to analyse and quantify biophysical metrics of subpopulations of cells in different states (Honrado et al., 2022). In this way, the proposed system can be used on unknown datasets, enabling an automated approach without the need for human intervention. Wang et al. coupled a deep learning model and code multiplexed MCCs network to enhance electrical waveform processing ability, and the trained neural networks not only recognised sensors' specific waveform patterns but also analysed interference between them (Fig. 6D) (Wang et al., 2019). This platform also possessed the capability to recognise particle size, measure speed, and locate the position.

3.2. Magnetic methods

3.2.1. Mechanism

Magnetic-based detection methods replace fluorescent beads and optical detectors, used in traditional devices, with magnetic beads (MBs) and magnetic sensors. In a magnetic-based detection process, MBs are dispersed in a fluid flowing inside a microchannel and detected by specialised magnetic sensors. Magnetic sensors detect the stray magnetic fields induced by flowing MBs and convert magnetic signals into electrical signals. The platform can record information (e.g., volume, velocity, and quantity) carried by target particles. In addition to basic measurement capabilities, the microfluidic platform also has the benefits of particle manipulation ability, an improvement of signal-to-noise ratio, and it also provides a negligible background with the help of the intrinsic properties of MBs.

Magnetic methods can be divided into several different types. Hall effect sensors use the Lorentz force to perform the sensing process and have a large linear detection range. Magnetoresistance (MR) sensors use the spin-transport electronics sensing principle and have a higher sensitivity (50 times that of the Hall effect), but the linear detection range is compromised. Quartz crystal microbalance (QCM) for detecting immobilised MBs can convert small mass changes into frequency changes of the output electrical signal with very high sensitivity; however, QCM sensors required more complex peripherals for signal detection and processing that may affect the system integration.

3.2.2. Magnetoresistance sensors

Among all magnetic-based microfluidic bioparticle detection platforms, MR sensors are the most widely used. The MR effect is that the resistivity of the material itself changes with the presence of magnetic fields (Tsukada et al., 2016). When the carriers of metal or semiconductors move in a magnetic field, the MR effect is produced due to the Lorentz force generated by the change in the magnetic field.

The giant magnetoresistance (GMR) effect generally arises in structures formed by alternating thin layers of ferromagnetic and non-ferromagnetic materials (Ren et al., 2020). If the magnetisation directions of adjacent ferromagnetic layers are anti-parallel, electrons are scattered to varying degrees, resulting in a large resistance, which is much greater than the normal MR. Huang et al. proposed a GMR platform based on 8 × 10 individually addressable sensors (Fig. 7A) (Huang et al., 2020a). When MBs-labelled target particles flow through a GMR sensor, this causes a change in the resistance of the sensor, and information about particle size can be deduced using the time interval between the passage of particles through each sensor in the array. The platform can offer 95% accuracy in counting biomimetic models and 98% accuracy in the detection of aptamer based pancreatic cancer cells. The throughput of the platform varies from 37 to 2730 cells/min depending on the flow rate settings for different targets. Similarly, Reisbeck et al. presented a magnetic flow cytometer coupled with GMR techniques to reveal the information contained in the magnetic fingerprints of MB labelled single cells (Fig. 7B) (Reisbeck et al., 2016). This work used RBCs as a biological model to demonstrate the capability of the platform for precise measurement of cell size and to distinguish cell morphology. Furthermore, to enhance the performance of the magnetic flow cytometer for measuring analytes containing different concentrations of cells, the same group integrated an *in situ* magnetic cell focusing function to the previously developed system to realize practical clinical assays without the need for a sample dilution process (Reisbeck et al., 2018). As shown in Fig. 7C, the platform uses four sections of mechanical chevron structures in the microfluidic channel to guide magnetic particles to the detection area. The height (h_n), length (L_n), and surface fraction (A_n) in each section are different, with the purpose of enabling adaptive focusing of magnetic particles. Magnetophoresis and mechanical methods activate the fully magnetic integrated workflow. At first (t_0), the microfluidic channel is rapidly filled with particles, followed by setting the flow rate to zero at moment t_1, where a permanent magnet will pull the magnetic particles in the channel to the substrate surface. Then, the application of a small flow rate (Q_2) balances the magnetic and fluidic drag forces exerted on the magnetic particles to focus them to the centre of the channel, thereby allowing them to be detected by the GMR sensor.

Chicharo et al. developed an adaptable magnetic micro flow cytometer for sensing whole cells (Chicharo et al., 2018). The GMR sensors are configured at the bottom of the microfluidic channel to form the detection area, and the 3D hydrodynamic focusing system brings the target cells close to the sensor to enhance the discrimination of labelled cells. Moreover, Lin et al. proposed the first integrated, high-performance flexible microfluidic detection platform based on a GMR sensor, and the platform can be bent to a radius of 2 mm while maintaining its full detection capacity (Lin et al., 2014). The sensor in the flexible electromagnetic analytical platform is powered by a constant current and the voltage variations are recorded by a programmed multimeter. The platform uses a Wheatstone bridge to detect emulsion droplets travelling through the detection area in real time, while a lock-in amplifier powers the entire bridge and improves the signal-to-noise ratio of the differential voltage signal.

Liu et al. used superparamagnetic nanocrystals to form magnetic microstructures with shapes such as spheres, dumbbells, pears, and chains by the microfluidic assembling method (Liu et al., 2020). These distinctive shapes of magnetic microstructures have different magnetic

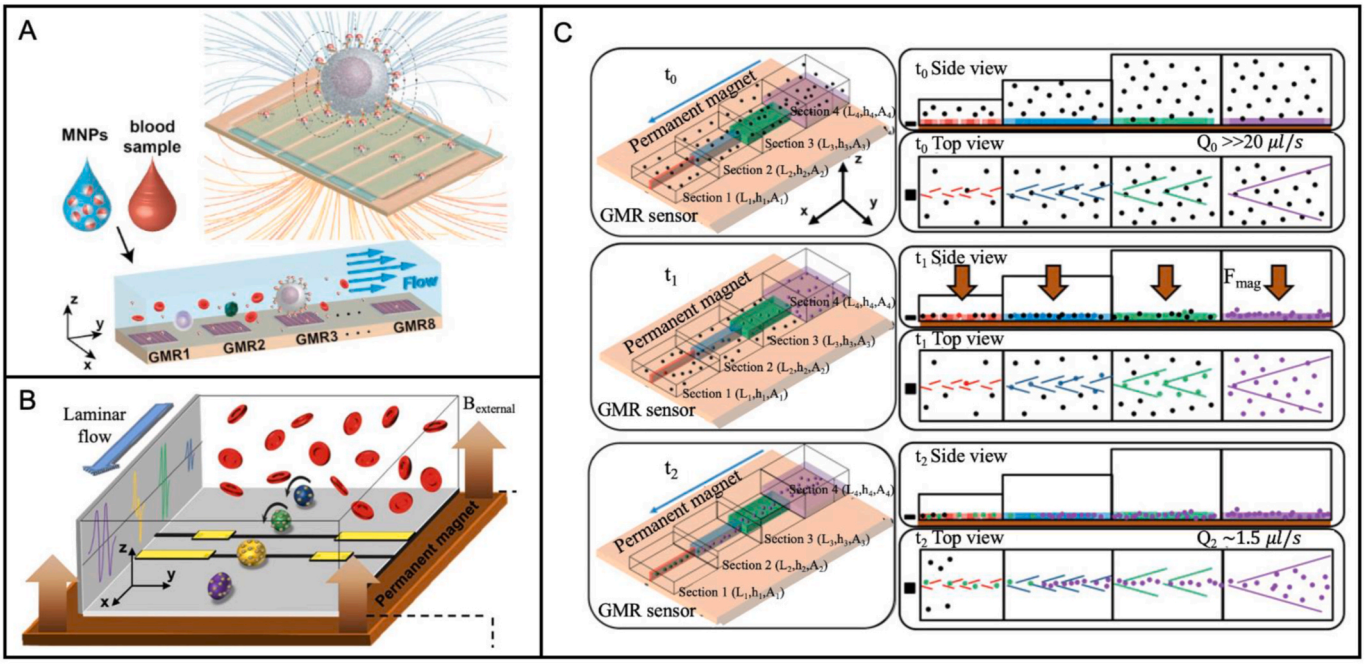

Fig. 7. Microfluidic MR sensor-based platforms. (A) Schematic of a GMR sensor array based magnetic microfluidic platform, where the time of passage of particles through each sensor can be recorded and used to analyse the results. Reproduced with permission (Huang et al., 2020a). Copyright 2020, Elsevier. (B) Schematic of a magnetic fingerprints based magnetic microfluidic platform. Reproduced with permission (Reisbeck et al., 2016). Copyright 2016, Springer Nature. (C) Schematic of a mechanical and magnetophoretic based magnetic microfluidic platform. The top, middle and bottom figures show the control and analysis of target particles by the microfluidic platform at different times (t_0, t_1, t_2). Reproduced with permission (Reisbeck et al., 2018). Copyright 2018, Elsevier.

fingerprints, which enable magnetic encoding and decoding. This work also designed a PDMS microfluidic platform based on the GMR sensor, and the whole system was able to successfully identify the characteristic peaks of the magnetic microstructures, thus realising the recognising function for the five target DNAs. Gao et al. proposed a portable microfluidic multi-biomarker detection platform based on a GMR sensor for clinical applications (Gao et al., 2019b). When the sample solution is added to the chamber, pressing the PDMS film causes the sample to oscillate back and forth in the channel, ensuring the complete dissolution of the labelled antibodies. Then, the mixture of the target and labelled antibodies is pumped to the surface of the GMR sensor, allowing them to be captured by the immunoreaction. Finally, the AC magnetic field is switched on and changes in the resistance of the GMR sensor are recorded. The proposed system can complete the simultaneous quantification of various protein biomarkers.

3.2.3. Other magnetic methods

In addition to MR/GMR based sensors, other magnetic sensors have been explored to detect and characterise cells. The Hall effect occurs when a current passes through a conductor in a magnetic field. The magnetic field generates a force on the electrons in the conductor perpendicular to the direction of electron movement, thus creating a potential difference in directions perpendicular to the conductor. Kim et al. combined the Hall and MR effect in a microfluidic platform and determined the resulting signal during the oscillation of 35 pL magnetic droplets (Kim et al., 2015). The on-chip magnetometer pushes the detection limit of samples to the picolitre range, solving limitations associated with Vibrating Sample Magnetometers (VSMs), and Superconducting Quantum Interference Devices (SQUIDs), which can only measure bulk liquid samples over a few microliters.

Moreover, Feng et al. integrated an immunoreaction chamber and a giant magnetoimpedance (GMI) sensor into a magnetic chip, thereby creating an integrated microfluidic platform for immunodetection of prostate specific antigen (PSA) (Feng et al., 2019). A GMI sensor detects changes in AC impedance through changes in the applied magnetic field in the conductor material. Functionalised immunomagnetic beads (IMBs) and PBS buffer are thoroughly mixed with the sample solution in the incubation chamber before entering the reactive chamber which contains pre-immobilised antibodies. The IMBs in the immunosandwich complexes produce stray magnetic fields, changing the signal strength in the GMI sensor. The limit of detection (LOD) of the chip can reach 0.1 ng/mL.

QCM is a very sensitive mass-measuring instrument that can reach nanogram accuracy. It uses the piezoelectric effect of quartz crystals to convert changes in the surface weight on the surface electrodes into changes in the resonant frequency as the output electrical signal. Han et al. integrated a QCM sensor into a microfluidic platform and demonstrated the detection of human immunoglobulin G (IgG) (Han et al., 2011). During the assay, the MBs exhibited two capabilities - the collection of target proteins and the amplification of the weight changes. The method showed a LOD of 0.1 ng/mL.

3.3. Acoustic methods

3.3.1. Mechanism

When acoustic waves enter a fluid, the particles dispersed in the fluid will be influenced by the acoustic radiation force (ARF) generated by the wave (Zhang et al., 2020). Acoustic standing waves can non-invasively manipulate objects at the microscopic scale, making it a promising technique for the controllable movement of bioparticles in microfluidic platforms (Ayan et al., 2016; Ozcelik et al., 2018). Acoustic standing waves are formed by superimposing two acoustic waves of the same frequency but with opposite propagation directions.

ARF acting on a compressible spherical object in a static acoustic field and a non-viscous fluid can be expressed as (Doinikov, 2006):

$$ARF = -\left(\frac{\pi p_0 V_p \beta_f}{2\lambda}\right)\varphi(\beta,\rho)sin\left(\frac{4\pi x}{\lambda}\right) \quad (6)$$

$$\varphi(\beta,\rho)=\frac{5\rho_p-2\rho_f}{2\rho_p+\rho_f}-\frac{\beta_p}{\beta_f} \tag{7}$$

where p_0 and V_p are the acoustic pressure and particle volume, respectively; subscripts f and p stand for fluid and particle, respectively; $\beta = 1/(\rho c^2)$ represents the compressibility where c is the speed of sound; ρ, λ and x represent density, wavelength, and distance from the pressure node, respectively; and φ represents the acoustic comparative coefficient. In an acoustic field, acoustic radiation forces affect almost all elastic particles, as long as the acoustic properties of the particles differ from those of the surrounding medium. For bioparticle detection, when target bioparticles enter the microfluidic channel, they are all guided by ARF to the acoustic pressure nodes or antinodes. By analysing trajectories and equilibrium positions, information such as the compressibility of bioparticles can be obtained.

Acoustic methods can be generally categorised based on the transducer used (IDTs or probes). Platforms using IDTs generate standing waves that can guide bioparticles in the microfluidic channel towards the acoustic pressure nodes or antinodes. By analysing trajectories and equilibrium positions, information such as the compressibility of bioparticles can be obtained. Platforms using acoustic probes, on the other hand, need much higher operating frequencies but can distinguish single particles.

3.3.2. *Detection methods based on interdigital acoustic transducers*

Several studies have shown that the mechanical properties of cells

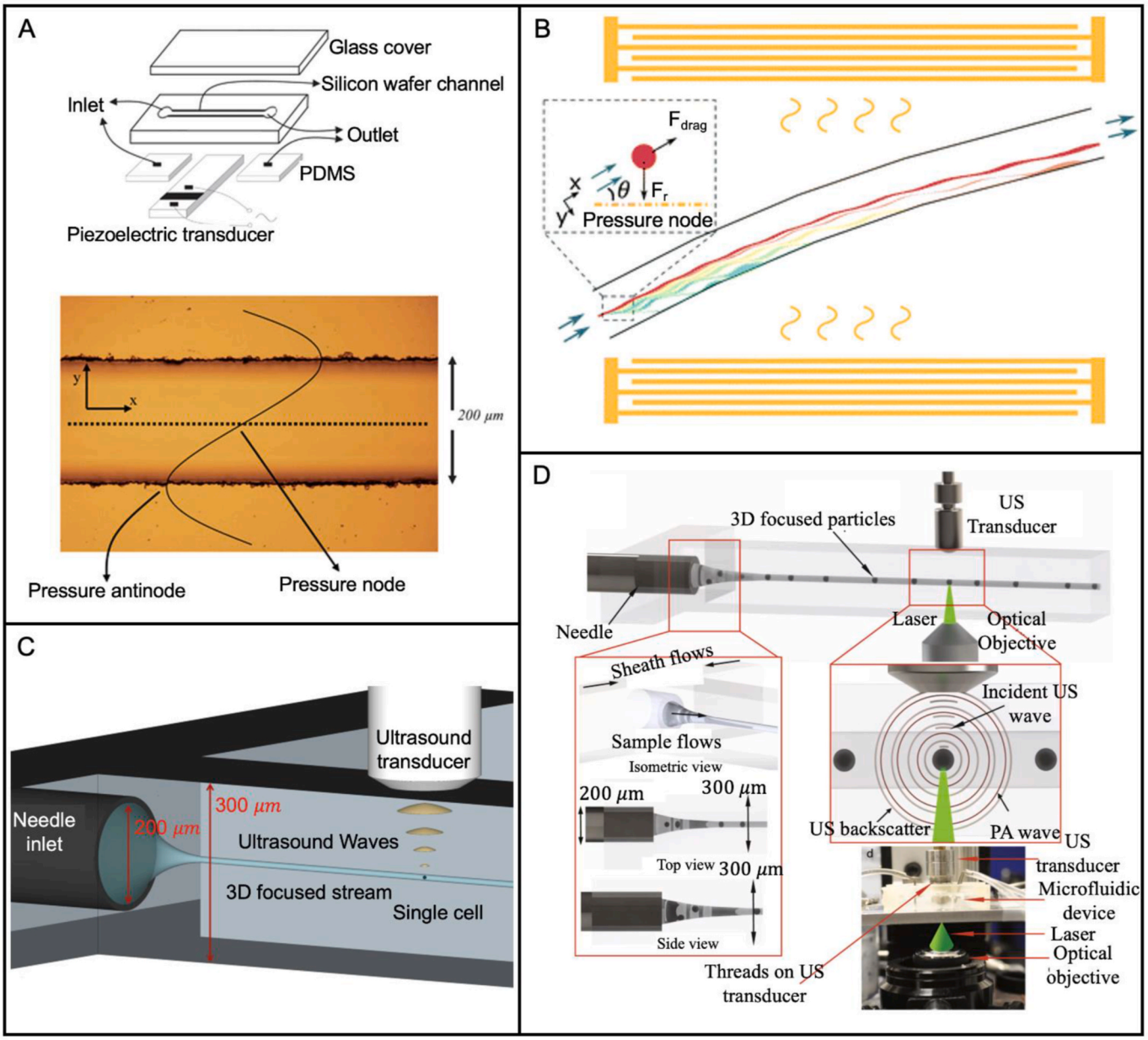

Fig. 8. Acoustic based microfluidic particle detection platforms. (A) Schematic of a contactless acoustic microfluidic platform. The acoustic chip used in the study (above) and image of channel with pressure antinode and pressure node (bottom). Reproduced with permission (Hartono et al., 2011). Copyright 2011, Royal Society of Chemistry. (B) Schematic of a multi-tilt surface acoustic waves based microfluidic platform. The platform enables separation of particles into different bins at different segments of the channel. Reproduced with permission (Wu et al., 2021). Copyright 2021, Royal Society of Chemistry. (C) Schematic of probe excited ultrasound based acoustic microfluidic platform. Cells are hydrodynamically focused to a narrow stream, and then flow through the transducer probe. Reproduced with permission (Strohm et al., 2019). Copyright 2019, Springer Nature. (D) Probe excited ultrasound and photoacoustic effect based acoustic microfluidic platform. Reproduced with permission (Gnyawali et al., 2019). Copyright 2019, Springer Nature.

are closely related to the pathological state of cells; for example, cancerous cells are softer than healthy cells (Remmerbach et al., 2009). Benefiting from the recent advancement of acoustic-based microfluidic technology, acoustic devices capable of analysing the mechanical properties of single cells have been developed. Standing acoustic waves are often used for acoustic based cell detection. Acoustic forces exerted on particles within the standing acoustic field guide them moving towards pressure nodes or antinodes based on their physical properties. Hartono et al. fabricated a contactless acoustic microfluidic chip for measuring the compressibility of biological cells (Hartono et al., 2011). As shown in Fig. 8A, the width of the microchannel depends on the acoustic half-wavelength. When standard polystyrene particles of known size are added into the channel together with unknown bioparticles (RBCs or cancer cells), samples are guided towards the acoustic pressure node by the ARF, and the trajectories of all particles are recorded during the process. Then, the acoustic energy density can be obtained from the physical properties (size, density, and compressibility) and trajectories of the polystyrene particles, thus inferring the compressibility of the target bioparticles. A further extension of this study was conducted by Wu et al., in which phase modulation of SAWs was used to pre-concentrate bioparticles on one line, and then new trajectories of biological particles were generated under the driving of ARF (Wu et al., 2019). However, the trajectory-based method needs to be implemented at low flow rates, which limits the throughput. To improve the throughput, Wu et al. developed a high-throughput microfluidic platform for cell compressibility measurement with multi-tilted SAWs, which can perform measurements on thousands of single cells in a few minutes (Wu et al., 2021). As shown in Fig. 8B, the detection area has a series of segments with varying angles with respect to the IDTs. As bioparticles move through the channel, due to their different physical properties, acoustic and hydrodynamic forces can drag them towards the sidewalls of different segments, thus separating them into different bins. Subsequent mathematical analysis enables the deduction of the compressibility of the bioparticles.

Moreover, Jeng et al. proposed a SAW sensor with a microfluidic channel to accomplish the detection of CRP (Jeng et al., 2021). The amplitude peak of the SAW sensor output signal varies with the increase in CRP concentration due to mass variation, and the peak shift shows a good linear relationship with the CRP concentration. The proposed platform can reach a LOD of 4 ng/mL.

3.3.3. Detection methods based on acoustic probes

The study of acoustic wave scattering from spherical objects in fluidic media was pioneered by Anderson as early as 1950 (Anderson, 1950), and the theory was subsequently refined over the following period. Based on this concept, when the particle size and acoustic wavelength are close in value, the generation of scattered waves depends largely on the particle volume. Different sizes and types of particles have unique acoustic characteristics that can enable identification and detection. Komatsu et al. proposed a diagnostic approach called 'sonocytometry', which uses reflections of high-frequency ultrasound to diagnose blood cells (Yosuke Komatsu et al., 2014). In this study, an ultrasonic transducer with a central frequency of 30 MHz is used to obtain ultrasonic backscatter signals from polystyrene particles (diameter of 80 or 100 μm). By increasing the sound wave frequency to 200 MHz, Strohm et al. achieved the detection of 6 and 10 μm diameter microparticles. However, the frequencies used in the above two platforms are too low to characterise biological cells (Strohm et al., 2014). Strohm et al. raised the ultrasound frequency to 375 MHz to reduce the acoustic wavelength to 4 μm in water, which is comparable to or even smaller than the size of a cell (Strohm et al., 2019). As shown in Fig. 8C, after 3D hydrodynamic focusing, the target particles come to the detection area. By comparing the spectral signatures obtained from the experiment with the given theoretical model, this work analysed acute myelogenous leukemia cells (10.0 ± 1.7 μm) and HT29 colorectal cancer cells (15.0 ± 2.3 μm).

Furthermore, when a pulsed laser is applied to a biological cell, the light-absorbing domain of the cell will generate an ultrasonic signal, which is known as the photoacoustic signal (Somer et al., 2020). The combination of backscattering and photoacoustics in a microfluidic platform enables label-free and multiparametric analysis. The backscattering features can provide information on cell size, morphology, and structure. Additionally, the light energy absorption state can give intracellular information on components such as lipids and mitochondria (Favazza et al., 2011). Gnyawali et al. integrated microfluidic, ultrasonic, and laser modules into a platform for the simultaneous analysis of particles using both acoustics and photoacoustics (Gnyawali et al., 2019). As shown in Fig. 8D, this platform can obtain multiple trait parameters from a single cell at the same time, such as physical and morphological features from ultrasound scattering, and optical absorption features from photoacoustic waves.

4. Conclusion and perspectives

The characterisation of biological and physical properties at the single bioparticle level is expected to provide a novel method for early diagnosis and prognostic assessment of diseases. With the continuous improvement of microfabrication and microelectronics technologies, the advantages of non-optical detection approach based microfluidic platforms are gradually emerging in the development of a new generation of portable, cost effective and convenient POCT devices. A highly integrated, fully automated, and cost-effective system with a robust bioparticle detection technique is essential to provide a promising solution to expand proof-of-concept systems in the lab to the automated clinical POCT devices of the future (Lin et al., 2022). To this end, this review has summarised recent advances in microfluidic particle detection platforms based on three non-optical detection methods, including electrical, magnetic, and acoustic. Methods for manipulating particles that are important for subsequent bioparticle detection have also been summarised.

Although non-optical microfluidic platforms have the potential to be further developed for clinical diagnostics, the following issues remain to be addressed in order to enable their full capabilities to be unlocked:

- Electrical methods need function generators, amplifiers, and PCs with user interfaces that can display/analyse the signal as separate components to work, which limits the portability and increases the cost of the system. Particularly, AC impedance flow cytometry systems often require lock-in amplifiers with a large bandwidth (operating frequency from a few kHz to hundreds of MHz) to provide sufficient capability for bioparticle detection and recognition. However, such amplifiers are bulky and expensive, making it challenging to achieve system integration at a low cost. High performance bioparticle detection platforms based on low-frequency AC impedance flow cytometry are yet to be developed. Using lock-in amplifiers is similar to the synchronous detection technique, in which both methods use signal demodulation. It is, therefore, possible to use diode envelope detectors with simpler designs at lower costs to extract result signals (Mei et al., 2012).
- Magnetic methods require permanent magnets or electromagnets and peripherals such as MR/GMR, Hall effect, and QCM sensors specialised for magnetic sensing, leading to bulky and complex operation of magnetic platforms. Most bioparticles are non-magnetic; therefore, magnetic labelling processes are required using monodisperse and highly magneto-responsive MBs, which are complex and expensive to prepare. Magnetotactic bacteria can move towards magnetic field lines under an external magnetic field, which is mainly due to the biosynthesis of magnetic nanoparticle chains (magnetosomes) within these bacteria (Gareev et al., 2021). Compared with conventional MBs, magnetosomes may possess the potential to reduce the cost and offer better biocompatibility and

therefore can be used as an alternative for producing higher performance sensing probes.

- For acoustic methods, high frequency devices are needed to shorten the wavelength of acoustic waves for bioparticle detection. This leads to the requirement of high frequency signal generators and power amplifiers with large bandwidths, which are bulky and expensive, making system integration difficult. Also, signal attenuation effects caused by soft materials such as polydimethylsiloxane (PDMS) at high frequencies can have a negative impact during the detection process. Although it is challenging to overcome the physical limitation of acoustic methods due to the nature of the detection mechanism, coating the bioparticle with materials (e.g., diamond nanoparticles) that can increase the acoustic contrast factor (thereby the ARF) may help increase the sensitivity and reduce system complexity (Raeymaekers et al., 2011).

Commercial optical flow cytometers are regarded as the current gold standard for clinical single cell analysis. The detection throughput, analysis speed, fluorescence resolution and sensitivity are the key indicators for judging the performance of related devices. Although non-optical microfluidic detection strategies have been shown to provide extensive information about bioparticles, their sensitivity and specificity are far from established commercial devices that use optical (fluorescent and scattering) technologies. To overcome this problem, future studies should focus on integrating different technologies (e.g., impedance sensors, magnetic sensors, and acoustic modules) to obtain more biological information. Full exploitation of the key benefits of non-optical microfluidic bioparticle detection methods will enable the development of low-cost POCT devices that are field deployable yet with sufficient capability for detection, supplementing existing optical based platforms.

Declaration of competing interest

The authors declare that they have no known competing financial interests or personal relationships that could have appeared to influence the work reported in this paper.

Data availability

Data will be made available on request.

Acknowledgements

This research received no external funding.

References

Alnaimat, F., Dagher, S., Mathew, B., Hilal-Alnqbi, A., Khashan, S., 2018. Chem. Rec. 18 (11), 1596–1612.
Amar, L.I., Hill, M.I., Faria, M., Guisado, D., van Rijn, C.J.M., Leonard, E.F., 2019. Biomed. Microdevices 21 (1), 12.
Amini, H., Lee, W., Di Carlo, D., 2014. Lab Chip 14 (15), 2739–2761.
Anderson, V.C., 1950. Acoustical Society of America 22 (4), 426–431.
Ayan, B., Ozcelik, A., Bachman, H., Tang, S.Y., Xie, Y., Wu, M., Li, P., Huang, T.J., 2016. Lab Chip 16 (22), 4366–4372.
Ayliffe, H.E.F.A.B., Rabbitt, R.D., 1999. J. Microelectromech. Syst. 8 (1), 50–57.
Bain, B.J., 2017. Medicine 45 (4), 187–193.
Bansal, M., 2020. Diabetes Metabol. Syndr. 14 (3), 247–250.
Battat, S., Weitz, D.A., Whitesides, G.M., 2022. Lab Chip 22 (3), 530–536.
Bellagambi, F.G., Lomonaco, T., Salvo, P., Vivaldi, F., Hangouët, M., Ghimenti, S., Biagini, D., Di Francesco, F., Fuoco, R., Errachid, A., 2020. TrAC, Trends Anal. Chem. 124, 115781.
Berli, C.L.A., 2007. Microfluid. Nanofluidics 4 (5), 391–399.
Blasi, T., Hennig, H., Summers, H.D., Theis, F.J., Cerveira, J., Patterson, J.O., Davies, D., Filby, A., Carpenter, A.E., Rees, P., 2016. Nat. Commun. 7 (1), 10256.
Brazey, B., Cottet, J., Bolopion, A., Van Lintel, H., Renaud, P., Gauthier, M., 2018. Lab Chip 18 (5), 818–831.
Caselli, F., De Ninno, A., Reale, R., Businaro, L., Bisegna, P., 2018. Sensor. Actuator. B Chem. 256, 580–589, 2018.
Cetin, B., Li, D., 2011. Electrophoresis 32 (18), 2410–2427.
Chandrasekaran, A., Packirisamy, M., 2010. Biomed. Microdevices 12 (5), 923–933.
Chen, Z., Liu, P., Zhao, X., Huang, L., Xiao, Y., Zhang, Y., Zhang, J., Hao, N., 2021. Appl. Mater. Today 25, 101239.
Cheng, Y., Ye, X., Ma, Z., Xie, S., Wang, W., 2016. Biomicrofluidics 10 (1), 014118.
Cheung, K., Gawad, S., Renaud, P., 2005. Cytometry 65 (2), 124–132.
Cheung, K.C., Di Berardino, M., Schade-Kampmann, G., Hebeisen, M., Pierzchalski, A., Bocsi, J., Mittag, A., Tarnok, A., 2010. Cytometry 77 (7), 648–666.
Chicharo, A., Martins, M., Barnsley, L.C., Taouallah, A., Fernandes, J., Silva, B.F.B., Cardoso, S., Dieguez, L., Espina, B., Freitas, P.P., 2018. Lab Chip 18 (17), 2593–2603.
Choi, H., Jeon, C.S., Hwang, I., Ko, J., Lee, S., Choo, J., Boo, J.H., Kim, H.C., Chung, T.D., 2014. Lab Chip 14 (13), 2327–2333.
Chun, H., Chung, Taek Dong, Kim, Hee Chan, 2005. Anal. Chem. 77 (8), 2490–2495.
Constantinou, I., Jendrusch, M., Aspert, T., Gorlitz, F., Schulze, A., Charvin, G., Knop, M., 2019. Micromachines 10 (5), 311.
Cottet, J., Kehren, A., van Lintel, H., Buret, F., Frénéa-Robin, M., Renaud, P., 2019. Microfluid. Nanofluidics 23 (1), 11.
Daguerre, H., Solsona, M., Cottet, J., Gauthier, M., Renaud, P., Bolopion, A., 2020. Lab Chip 20 (20), 3665–3689.
De Stefano, P., Bianchi, E., Dubini, G., 2022. Biomicrofluidics 16 (3), 031501.
Doinikov, A.A., 2006. J. Fluid Mech. 267, 1017.
Fan, Y., Dong, D., Li, Q., Si, H., Pei, H., Li, L., Tang, B., 2018. Lab Chip 18 (8), 1151–1173.
Favazza, C.P., Cornelius, L.A., Wang, L.V., 2011. J. Biomed. Opt. 16 (2), 026004.
Feng, Z., Zhi, S., Guo, L., Zhou, Y., Lei, C., 2019. Mikrochim. Acta 186 (4), 252.
Furniturewalla, A., Chan, M., Sui, J., Ahuja, K., Javanmard, M., 2018. Microsyst Nanoeng 4 (1), 1–10.
Gao, B., Yang, Y., Liao, J., He, B., Liu, H., 2019a. Lab Chip 19 (21), 3602–3608.
Gao, W., Saqib, M., Qi, L., Zhang, W., Xu, G., 2017. Current Opinion in Electrochemistry 3 (1), 4–10.
Gao, Y., Huo, W., Zhang, L., Lian, J., Tao, W., Song, C., Tang, J., Shi, S., Gao, Y., 2019b. Biosens. Bioelectron. 123, 204–210.
Gao, Y., Wu, M., Lin, Y., Xu, J., 2020. Micromachines 11 (10), 921.
Gareev, K.G., Grouzdev, D.S., Kharitonskii, P.V., Kosterov, A., Koziaeva, V.V., Sergienko, E.S., Shevtsov, M.A., 2021. Magnetochemistry 7 (6), 86.
Gautam, S., Hens, L., 2020. COVID-19: impact by and on the environment, health and economy. Environ. Dev. Sustain. 22 (6), 4953–4954.
Gawad, S., Schild, L., Renaud, P.H., 2001. Lab Chip 1 (1), 76–82.
Gnyawali, V., Strohm, E.M., Wang, J.Z., Tsai, S.S.H., Kolios, M.C., 2019. Sci. Rep. 9 (1), 4775.
Gong, Y., Fan, N., Yang, X., Peng, B., Jiang, H., 2018. New advances in microfluidic flow cytometry. Electrophoresis 40 (8), 1212–1229.
Haandbaek, N., Burgel, S.C., Heer, F., Hierlemann, A., 2014a. Lab Chip 14 (2), 369–377.
Haandbaek, N., With, O., Burgel, S.C., Heer, F., Hierlemann, A., 2014b. Lab Chip 14 (17), 3313–3324.
Hamacher, T., Berendsen, J.T.W., van Dongen, J.E., van der Hee, R.M., Cornelissen, J., Broekhuijse, M., Segerink, L.I., 2021. Lab Chip 21 (22), 4477–4486.
Hamza, B., Ng, S.R., Prakadan, S.M., Delgado, F.F., Chin, C.R., King, E.M., Yang, L.F., Davidson, S.M., DeGouveia, K.L., Cermak, N., Navia, A.W., Winter, P.S., Drake, R.S., Tammela, T., Li, C.M., Papagiannakopoulos, T., Gupta, A.J., Shaw Bagnall, J., Knudsen, S.M., Vander Heiden, M.G., Wasserman, S.C., Jacks, T., Shalek, A.K., Manalis, S.R., 2019. Proc. Natl. Acad. Sci. U.S.A. 116 (6), 2232–2236.
Han, J., Zhang, J., Xia, Y., Li, S., Jiang, L., 2011. Colloids Surf. A Physicochem. Eng. Asp. 379 (1–3), 2–9.
Harper, L., Kalfa, N., Beckers, G.M.A., Kaefer, M., Nieuwhof-Leppink, A.J., Fossum, M., Herbst, K.W., Bagli, D., Committee, E.R., 2020. J. Pediatr. Urol. 16 (5), 715–716.
Hartono, D., Liu, Y., Tan, P.L., Then, X.Y., Yung, L.Y., Lim, K.M., 2011. Lab Chip 11 (23), 4072–4080.
Hejazian, M., Li, W., Nguyen, N.T., 2015. Lab Chip 15 (4), 959–970.
Heo, Y.J., Lee, D., Kang, J., Lee, K., Chung, W.K., 2017. Sci. Rep. 7 (1), 11651.
Hochstetter, A., Vernekar, R., Austin, R.H., Becker, H., Beech, J.P., Fedosov, D.A., Gompper, G., Kim, S.C., Smith, J.T., Stolovitzky, G., Tegenfeldt, J.O., Wunsch, B.H., Zeming, K.K., Kruger, T., Inglis, D.W., 2020. ACS Nano 14 (9), 10784–10795.
Honrado, C., McGrath, J.S., Reale, R., Bisegna, P., Swami, N.S., Caselli, F., 2020. Anal. Bioanal. Chem. 412 (16), 3835–3845.
Honrado, C., Salahi, A., Adair, S.J., Moore, J.H., Bauer, T.W., Swami, N.S., 2022. Lab Chip 22 (19), 3708–3720.
Huang, C.C., Ray, P., Chan, M., Zhou, X., Hall, D.A., 2020a. Biosens. Bioelectron. 169, 112362.
Huang, D., Man, J., Jiang, D., Zhao, J., Xiang, N., 2020b. Electrophoresis 41 (24), 2166–2187.
Huang, H.Y., Lai, Y.L., Yao, D.J., 2018. Micromachines 9 (3), 135.
Jeng, M.-J., Li, Y.-C., Sharma, M., Chen, C.-W., Tsai, C.-L., Lin, Y.-H., Huang, S.-F., Chang, L.-B., Lai, C.-S., 2021. Chemosensors 9 (5), 106.
Jung, W., Han, J., Choi, J.-W., Ahn, C.H., 2015. Microelectron. Eng. 132, 46–57.
Karakuzu, B., Gulmez, Y., Tekin, H.C., 2021. Microelectron. Eng. 247, 111583.
Kellman, M., Rivest, F., Pechacek, A., Sohn, L., Lustig, M., 2018. IEEE Sensor. J. 18 (8), 3068–3079.
Khoshmanesh, K., Nahavandi, S., Baratchi, S., Mitchell, A., Kalantar-zadeh, K., 2011. Biosens. Bioelectron. 26 (5), 1800–1814.
Kim, G.-Y., Han, J.-I., Park, J.-K., 2018. BioChip J. 12 (4), 257–267.
Kim, H., Kim, J., 2013. Microfluid. Nanofluidics 16 (4), 623–633.
Kim, K.W., Reddy, V., Torati, S.R., Hu, X.H., Sandhu, A., Kim, C.G., 2015. Lab Chip 15 (3), 696–703.
Kumar, A., Parihar, A., Panda, U., Parihar, D.S., 2022. ACS Appl. Bio Mater. 5 (5), 2046–2068.

Lang, T.C., Zhao, R., Kim, A., Wijewardena, A., Vandervord, J., McGrath, R., Fitzpatrick, S., Fulcher, G., Jackson, C.J., 2019. Burns 45 (7), 1659–1672.
Larsen, U.D.B.G., Branebjerg, J., 1997. Proceed. Int.Solid. State. Sensors. Actuators Conf. 2, 1319–1322.
Lee, J.H., Lee, H.S., Ahn, S.B., Kwon, Y.J., 2021a. Clin. Nutr. 40 (10), 5252–5260.
Lee, W.C., Ng, H.Y., Hou, C.Y., Lee, C.T., Fu, L.M., 2021b. Lab Chip 21 (8), 1433–1453.
Lenshof, A., Evander, M., Laurell, T., Nilsson, J., 2012. Lab Chip 12 (4), 684–695.
Li, C.-z., 2019. J. Anal. Test. 3 (1), 1–2.
Li, S., Ma, Z., Cao, Z., Pan, L., Shi, Y., 2020. Small 16 (9), 1903822.
Li, X., Fan, B., Liu, L., Chen, D., Cao, S., Men, D., Wang, J., Chen, J., 2018. Sci. Rep. 8 (1), 14229.
Lin, G., Makarov, D., Melzer, M., Si, W., Yan, C., Schmidt, O.G., 2014. Lab Chip 14 (20), 4050–4058.
Lin, H., Yu, W., K, A.S., Bogumil, M., Zhao, Y., Hambalek, J., Lin, S., Chandrasekaran, S., Garner, O., Di Carlo, D., Emaminejad, S., 2022. Nature 611, 570–577.
Liu, Y., Lin, G., Chen, Y., Monch, I., Makarov, D., Walsh, B.J., Jin, D., 2020. Lab Chip 20 (24), 4561–4571.
Lu, X., Xuan, X., 2015. Anal. Chem. 87 (12), 6389–6396.
Luo, L., He, Y., 2020. Cancer Med. 9 (12), 4207–4231.
Luppa, P.B., Muller, C., Schlichtiger, A., Schlebusch, H., 2011. Trends Anal. Chem. 30 (6), 887–898.
Mahesh, K., Varma, M., Sen, P., 2020. Lab Chip 20 (22), 4296–4309.
Mansor, M., Takeuchi, M., Nakajima, M., Hasegawa, Y., Ahmad, M., 2017. Appl. Sci. 7 (2), 170.
Mei, Z., Cho, S.H., Zhang, A., Dai, J., Wu, T.-F., Lo, Y.-H., 2012. 2012 Annual International Conference of the IEEE Engineering in Medicine and Biology Society, pp. 6277–6280.
Meier, S., Henkens, M., Heymans, S., Robinson, E.L., 2021. J Cardiovasc Transl Res 14 (1), 53–62.
Mok, J., Mindrinos, M.N., Davis, R.W., Javanmard, M., 2014. Proc. Natl. Acad. Sci. U. S. A. 111 (6), 2110–2115.
Morgan, H., Green, N.G., 2003. Research Studies Press.
Morijiri, T., Sunahiro, S., Senaha, M., Yamada, M., Seki, M., 2011. Microfluid. Nanofluidics 11 (1), 105–110.
Murakami, T., Koiwai, K., Suzuki, H., 2021. Sensor. Actuator. B Chem. 347, 130587.
Nakano, M., Ding, Z., Matsuda, K., Xu, J., Inaba, M., Suehiro, J., 2019. Biomicrofluidics 13 (6), 064109.
Nasir, N., Al Ahmad, M., 2020. J. Eng., 9475490, 2020.
Nguyen, H.T., Thach, H., Roy, E., Huynh, K., Perrault, C.M., 2018. Micromachines 9 (9), 461.
Ozcelik, A., Rich, J., Huang, T.J., 2022. Multidisciplinary Microfluidic and Nanofluidic Lab-On-A-Chip, pp. 297–321.
Ozcelik, A., Rufo, J., Guo, F., Gu, Y., Li, P., Lata, J., Huang, T.J., 2018. Nat. Methods 15 (12), 1021–1028.
Pallazola, V.A., Davis, D.M., Whelton, S.P., Cardoso, R., Latina, J.M., Michos, E.D., Sarkar, S., Blumenthal, R.S., Arnett, D.K., Stone, N.J., Welty, F.K., 2019. Mayo Clin Proc Innov Qual Outcomes 3 (3), 251–267.
Panwar, J., Roy, R., 2019. Microelectron. Eng. 215, 111010.
Patterson, E., Ryan, P.M., Cryan, J.F., Dinan, T.G., Ross, R.P., Fitzgerald, G.F., Stanton, C., 2016. Postgrad. Med. 92 (1087), 286–300.
Pokhrel, S., Chhetri, R., 2021. Higher Education for the Future 8 (1), 133–141.
Raeymaekers, B., Pantea, C., Sinha, D.N., 2011. J. Appl. Phys. 109 (1), 014317.
Ramirez-Murillo, C.J., de Los Santos-Ramirez, J.M., Perez-Gonzalez, V.H., 2021. Electrophoresis 42 (5), 565–587.
Reisbeck, M., Helou, M.J., Richter, L., Kappes, B., Friedrich, O., Hayden, O., 2016. Sci. Rep. 6 (1), 32838.
Reisbeck, M., Richter, L., Helou, M.J., Arlinghaus, S., Anton, B., van Dommelen, I., Nitzsche, M., Bassler, M., Kappes, B., Friedrich, O., Hayden, O., 2018. Biosens. Bioelectron. 109, 98–108.
Remmerbach, T.W., Wottawah, F., Dietrich, J., Lincoln, B., Wittekind, C., Guck, J., 2009. Cancer Res. 69 (5), 1728–1732.
Ren, C., Bayin, Q., Feng, S., Fu, Y., Ma, X., Guo, J., 2020. Biosens. Bioelectron. 165, 112340.
Reynard, C., Allen, J.A., Shinkins, B., Prestwich, G., Goves, J., Davies, K., Body, R., group, C., 2022. Emerg. Med. J. 39 (1), 70–76.
Rezaei, B., Moghimi Zand, M., Javidi, R., 2021. J. Chromatogr. A 1649, 462216.
Rodriguez-Trujillo, R., Castillo-Fernandez, O., Garrido, M., Arundell, M., Valencia, A., Gomila, G., 2008. Biosens. Bioelectron. 24 (2), 290–296.
Roth-Kleiner, M., Stadelmann Diaw, C., Urfer, J., Ruffieux, C., Werner, D., 2010. Eur. J. Pediatr. 169 (11), 1387–1395.
Sachdeva, S., Davis, R.W., Saha, A.K., 2020. Front. Bioeng. Biotechnol. 8, 602659.
Sherbaz, A., Konak, B.M.K., Pezeshkpour, P., Di Ventura, B., Rapp, B.E., 2022. Micromachines 13 (3), 365.
Sinha, A., Tai, T.Y., Li, K.H., Gopinathan, P., Chung, Y.D., Sarangadharan, I., Ma, H.P., Huang, P.C., Shiesh, S.C., Wang, Y.L., Lee, G.B., 2019. Biosens. Bioelectron. 129, 155–163.
Somer, A., Gonçalves, A., Moreno, T.V., Cruz, G.K.d., Baesso, M.L., Astrath, N.G.C., Novatski, A., 2020. Meas. Sci. Technol. 31 (7), 075202.
Song, Y., Zhang, J., Li, D., 2017. Micromachines 8 (7), 204.
Sotiropoulou, C.L., Voudouris, L., Gentsos, C., Demiris, A.M., Vassiliadis, N., Nikolaidis, S., 2014. IEEE Trans Biomed Circuits Syst 8 (2), 268–277.
Spencer, D., Caselli, F., Bisegna, P., Morgan, H., 2016. Lab Chip 16 (13), 2467–2473.
Spencer, D.C., Paton, T.F., Mulroney, K.T., Inglis, T.J.J., Sutton, J.M., Morgan, H., 2020. Nat. Commun. 11 (1), 5328.
Stavrakis, S., Holzner, G., Choo, J., deMello, A., 2019. Curr. Opin. Biotechnol. 55, 36–43.
Strohm, E.M., Gnyawali, V., Sebastian, J.A., Ngunjiri, R., Moore, M.J., Tsai, S.S.H., Kolios, M.C., 2019. Sci. Rep. 9 (1), 4775.
Strohm, E.M., Kolios, M.C., Hwang, D.K., Moon, B.U., Tsai, S.S., 2014. IEEE International Ultrasonics Symposium, pp. 1960–1963.
Sun, J., Gao, Y., Isaacs, R.J., Boelte, K.C., Lin, P.C., Boczko, E.M., Li, D., 2012. Anal. Chem. 84 (4), 2017–2024.
Tai, W.C., Chang, Y.C., Chou, D., Fu, L.M., 2021. Biosensors 11 (8), 260.
Tang, S.Y., Zhang, W., Baratchi, S., Nasabi, M., Kalantar-Zadeh, K., Khoshmanesh, K., 2013. Anal. Chem. 85 (13), 6364–6371.
Tang, T., Liu, X., Kiya, R., Shen, Y., Yuan, Y., Zhang, T., Suzuki, K., Tanaka, Y., Li, M., Hosokawa, Y., Yalikun, Y., 2021. Biosens. Bioelectron. 193, 113521.
Tang, W., Tang, D., Ni, Z., Xiang, N., Yi, H., 2017. Anal. Chem. 89 (5), 3154–3161.
Tao, Y., Shen, H., Deng, K., Zhang, H., Yang, C., 2021. Sensor. Actuator. B Chem. 339, 129730.
Tsukada, K., Haga, Y., Morita, K., Song, N., Sakai, K., Kiwa, T., Cheng, W., 2016. IEEE Trans. Magn. 52 (7), 6201504.
van Dinther, A.M.C., Schroën, C.G.P.H., Imhof, A., Vollebregt, H.M., Boom, R.M., 2013. Microfluid. Nanofluidics 15 (4), 451–465.
Vig, A.L., Kristensen, A., 2008. Appl. Phys. Lett. 93 (20), 203507.
Wang, H., Sobahi, N., Han, A., 2017. Lab Chip 17 (7), 1264–1269.
Wang, N., Liu, R., Asmare, N., Chu, C.H., Sarioglu, A.F., 2019. Lab Chip 19 (19), 3292–3304.
Wu, Y., Stewart, A.G., Lee, P.V.S., 2019. Biomicrofluidics 13 (2), 024107.
Wu, Y., Stewart, A.G., Lee, P.V.S., 2021. Lab Chip 21 (14), 2812–2824.
Wunsch, B.H., Smith, J.T., Gifford, S.M., Wang, C., Brink, M., Bruce, R.L., Austin, R.H., Stolovitzky, G., Astier, Y., 2016. Nat. Nanotechnol. 11 (11), 936–940.
Xavier, M., Holm, S.H., Beech, J.P., Spencer, D., Tegenfeldt, J.O., Oreffo, R.O.C., Morgan, H., 2019. Lab Chip 19 (3), 513–523.
Xiang, N., Chen, K., Dai, Q., Jiang, D., Sun, D., Ni, Z., 2014. Microfluid. Nanofluidics 18 (1), 29–39.
Xie, X., Zhang, Z., Ge, X., Zhao, X., Hao, L., Cheng, Z., Zhou, W., Du, Y., Wang, L., Tian, F., Xu, X., 2019. Anal. Chem. 91 (21), 13398–13406.
Yaman, S., Anil-Inevi, M., Ozcivici, E., Tekin, H.C., 2018. Front. Bioeng. Biotechnol. 6, 192.
Yan, J., Wang, C., Fu, Y., Guo, J., Guo, J., 2022. Analyst 147 (14), 3225–3233.
Yang, D., Ai, Y., 2019. Lab Chip 19 (21), 3609–3617.
Yang, L., Zhang, Z., Wang, X., 2022. Micromachines 13 (4), 552.
Yosuke Komatsu, R.N., Ken-ichi, Funamoto, Hayase, Toshiyuki, Masauzi, Nobuo, Kanai, Hiroshi, Saijo, Yoshifumi, 2014. 36th Annual International Conference of the IEEE Engineering in Medicine and Biology Society, pp. 2761–2764.
Zhang, H., Chang, H., Neuzil, P., 2019a. Micromachines 10 (6), 423.
Zhang, L., Ding, B., Chen, Q., Feng, Q., Lin, L., Sun, J., 2017a. TrAC, Trends Anal. Chem. 94, 106–116.
Zhang, P., Bachman, H., Ozcelik, A., Huang, T.J., 2020. Annu. Rev. Anal. Chem. 13 (1), 17–43.
Zhang, Q., Li, Z., Zhao, S., Wen, W., Chang, L., Yu, H., Jiang, T., 2017b. Cytometry 91 (2), 126–132.
Zhang, W., Hu, Y., Choi, G., Liang, S., Liu, M., Guan, W., 2019b. Sensor. Actuator. B Chem. 296, 126615.
Zhao, Q., Yuan, D., Zhang, J., Li, W., 2020. Micromachines 11 (5), 461.
Zheng, J., Cole, T., Zhang, Y., Kim, J., Tang, S.Y., 2021. Biosens. Bioelectron. 194, 113666.
Zheng, S., Liu, M., Tai, Y.C., 2008. Biomed. Microdevices 10 (2), 221–231.
Zhou, X., Liang, X.M., Wang, J., Du, P., Gao, D., 2018. Int. J. Heat Mass Tran. 127, 637–644.
Zhu, Z., Chen, W., Tian, B., Luo, Y., Lan, J., Wu, D., Chen, D., Wang, Z., Pan, D., 2018. Sensor. Actuator. B Chem. 275, 470–482.